Late Paleozoic Accretionary and Collisional Processes along the Southern Peri-Siberian Orogenic System: New Constraints from Amphibolites within the Irtysh Complex of Chinese Altai

Ming Chen,[1,2,*] *Min Sun,*[2] *Pengfei Li,*[3] *Jianping Zheng,*[1] *Keda Cai,*[4] *and Yuping Su*[1]

1. School of Earth Sciences, China University of Geosciences, Wuhan 430074, China; 2. Department of Earth Sciences, University of Hong Kong, Pokfulam Road, Hong Kong, China; 3. State Key Laboratory of Isotope Geochemistry, Guangzhou Institute of Geochemistry, Chinese Academy of Sciences, Guangzhou 510640, China; 4. School of Earth Sciences and Resources, China University of Geosciences, Beijing 100083, China

ABSTRACT

The Irtysh shear zone is one of the largest strike-slip systems within the Central Asian Orogenic Belt, recording the accretionary-collisional processes between the peri-Siberian and Kazakhstan-Junggar orogenic systems. This study focuses mainly on amphibolites from the Irtysh Complex, the best-preserved exposure of the shear zone in northwestern China. Their protoliths and metamorphic ages/conditions are investigated to constrain the tectonic affinity of this complex and to explore the above-mentioned tectonic processes. Three types of amphibolites are identified geochemically. The geochemical compositions of type I suggest that their protoliths represent N-MORB (normal mid-ocean ridge basalt)-type basalts that could be produced by ca. 10% partial melting of depleted spinel lherzolites. Type II amphibolites are characterized by enriched-MORB-type trace-element signatures. Their protoliths were possibly generated by <5% partial melting of a similar mantle source. Type III amphibolites show typical arc affinity and have a more depleted mantle source. We infer that ankaramites from the Dulate arc of East Junggar, part of the Kazakhstan-Junggar orogenic system, possibly served as their protoliths. The available data suggest that the Irtysh Complex probably represents an accretionary complex built along the southern Chinese Altai (part of the peri-Siberian orogenic system), incorporating crustal relicts from both the Ob-Zaisan Ocean and the Dulate arc. Metamorphic investigation shows that the amphibolite facies metamorphism occurred at ca. 284 Ma, recording a high geothermal gradient (30°–45°C/km) along the Irtysh shear zone. Data compilation suggests that East Junggar probably collided with Chinese Altai between ca. 313 and 299 Ma, which was followed by an episode of high- to ultrahigh-temperature metamorphism possibly related to syn-/postcollisional extension in the early Permian.

Online enhancements: appendix figure and tables.

Introduction

Accretionary orogens form along convergent margins and are characterized by relatively long-lived arc magmatism as well as incorporation of continental/oceanic fragments (e.g., Matsuda and Uyeda 1971; Maruyama 1997; Cawood et al. 2009). Such orogens have formed since the early Proterozoic or even the Archean and are of great importance in understanding crustal growth and differentiation (Jahn 2004; Condie 2007; Condie and Kröner 2008; Cawood et al. 2009). The Central Asian Orogenic Belt (CAOB), bordered by the Siberian continent to the north and the Tarim–North China continent to the south (fig. 1 inset), represents the largest Phanerozoic accretionary orogenic belt and thus serves an ideal example in exploring the mechanism of accretionary orogenesis (Şengör et al. 1993; Windley et al. 2007; Xiao et al. 2009, 2010). Previous studies have revealed that this huge orogenic collage consists mainly of diverse magmatic arcs, fore-/backarc basins, accretion-

Manuscript received April 6, 2018; accepted September 14, 2018; electronically published January 14, 2019.

* Author for correspondence; email: chm.881028@163.com, chm.881028@gmail.com.

[The Journal of Geology, 2019 volume 127, p. 241–262] 0022-1376/2019/12702-0007$15.00. DOI: 10.1086/701253

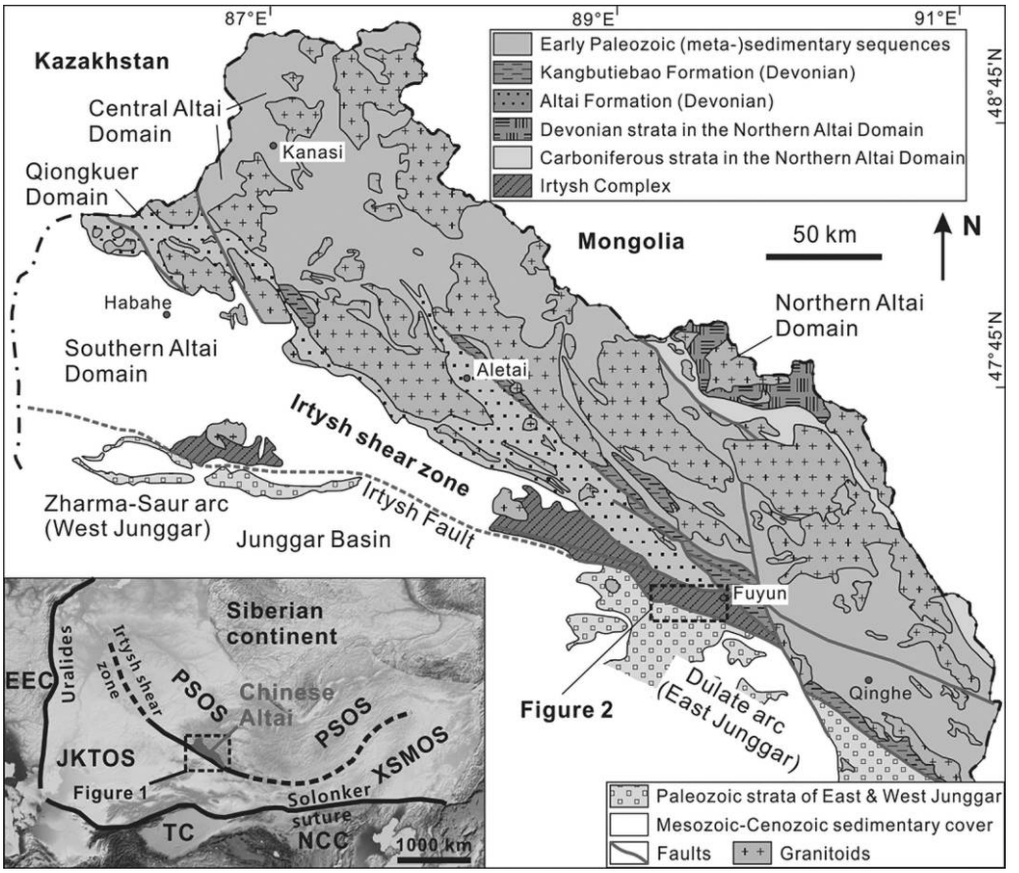

Figure 1. Simplified geological map showing the architecture of Chinese Altai and adjacent East/West Junggar (modified after Li et al. 2017). The inset shows that the Central Asian Orogenic Belt, between the Siberian continent to the north and the Tarim and North China continents to the south, is composed of the peri-Siberian orogenic system (PSOS) in the north, the Junggar-Kazakhstan-Tianshan orogenic system (JKTOS) in the southwest, and the Xing'an–South Mongolia orogenic system (XSMOS) in the southeast. EEC = East European continent; TC = Tarim continent; NCC = North China continent. A color version of this figure is available online.

ary prisms, ophiolites, and minor microcontinents, which were brought together through multiple episodes of subduction-accretion of the Paleo-Asian Ocean from the latest Mesoproterozoic to the late Paleozoic (Zonenshain et al. 1990; Şengör et al. 1993; Khain et al. 2003; Jahn 2004; Windley et al. 2007; Xiao et al. 2010, 2015, 2018; Wilhem et al. 2012; Eizenhöfer and Zhao 2018; Han and Zhao 2018). The consumption of diverse branches of this giant ocean formed a number of suture zones in the CAOB (e.g., Demoux et al. 2009; Jian et al. 2014; Xiao et al. 2014; Han and Zhao 2018). In the late Paleozoic, the final collision between the Tarim–North China and Siberian continents reactivated these suture zones and caused intense strike-slip faulting and/or thrusting, giving rise to numerous strike-slip shear zones (Buslov et al. 2001, 2004; Laurent-Charvet et al. 2003; Briggs et al. 2007; Li et al. 2015*a*, 2015*b*, 2016*a*, 2016*b*, 2017). Distinguishing among various subduction-accretion processes and subsequent collision-induced deformation along these shear zones is therefore central to understanding the tectonic evolution and crustal growth in the CAOB.

The Irtysh shear zone, extending from northeastern Kazakhstan to northwestern China (fig. 1 inset), is one of the largest strike-slip systems in the CAOB (Coleman 1989; Zonenshain et al. 1990; Buslov et al. 2001, 2004; Zhang et al. 2012; Xiao et al. 2014; Li et al. 2017). This tectonic belt is considered to record the accretionary and collisional processes between the active margin of the Siberian continent to the north (e.g., the Altai Orogen; Wang et al. 2006, 2009*a*; Yuan et al. 2007; Sun et al. 2008, 2009*b*; Cai et al. 2010, 2011, 2012; Long et al. 2010; Chen et al. 2014, 2015*a*, 2015*b*, 2016*a*, 2016*b*; Jiang et al. 2016, 2017) and the Kazakhstan-Junggar orogenic collage (e.g., the Dulate arc of East Junggar) to the south (Dobretsov et al. 1995; Buslov et al. 2001, 2004; Z. Zhang et al. 2008, 2009; Su et al. 2012; C. Zhang et al. 2012). Some researchers proposed that the peri-Siberian oro-

genic system was still under subduction of an oceanic plate in the late Carboniferous, generating arc-type igneous rocks (e.g., Cai et al. 2012), and that its collision with the Kazakhstan-Junggar orogenic system took place before the earliest Permian (Zhang et al. 2012; Gao and Zhou 2013; Li et al. 2015*a*, 2017). Other researchers argued that the amalgamation of these two orogenic systems possibly occurred in the Late Devonian, followed by postcollision magmatism and tectonics in the Carboniferous to early Permian (Liu et al. 2012; Tong et al. 2012; Hong et al. 2017). We note that most of these studies were focused mainly on the granitoids emplaced along the Irtysh shear zone and that the geochemistry of these rocks might lead to uncertainties in tectonic interpretation. Previous field investigations revealed the diversity of lithologies within the Irtysh shear zone, including ophiolitic mélanges and various types of metamorphic rocks (e.g., amphibolites, schists, and gneisses), all of which are characterized by strong deformation and high-grade metamorphism (He et al. 1990; Qu and Zhang 1991; Laurent-Charvet et al. 2003; Briggs et al. 2007; Xiao et al. 2009; Wang et al. 2012; Li et al. 2015*a*, 2017). Understanding their protolith nature, metamorphic conditions, and deformation history can provide more thorough constraints on the accretionary and collisional processes between the peri-Siberian and Kazakhstan-Junggar orogenic systems (Li et al. 2015*a*, 2017). In particular, the Irtysh Complex in northwestern China represents one of the best exposures of the Irtysh shear zone, therefore possibly providing unique insights into these tectonic processes. Nevertheless, because of the scarcity of high-quality geochemical and geochronological data, the origin of the diverse rock types within this complex has been poorly constrained, leading to ambiguities of tectonic interpretation (e.g., Qu and Zhang 1991; O'Hara et al. 1997; Windley et al. 2002; Xiao et al. 2009).

In this study, we mainly focus on the amphibolites from the Irtysh Complex. Combined zircon U-Pb dating and mineral/whole-rock geochemical investigations were conducted to reveal their protoliths as well as metamorphic ages and conditions. These new data, together with recent structural analyses (Li et al. 2015*a*, 2017), enable us to constrain the tectonic affinity of the Irtysh Complex and to more thoroughly decipher the tectonic and metamorphic evolution of the Irtysh shear zone. These, in turn, enhance our understanding of orogenic processes and architecture of the western CAOB.

Geological Setting

The CAOB can be subdivided into the peri-Siberian orogenic system in the north, the Junggar-Kazakhstan-Tianshan orogenic system in the southwest, and the Xing'an–South Mongolia orogenic system in the southeast (Wilhem et al. 2012; Xiao et al. 2015; Li et al. 2017; fig. 1 inset). The formation of these three systems can be attributed to multiple Neoproterozoic to late Paleozoic subduction-accretion processes surrounding the southern Siberian continent, the microcontinents of Kazakhstan-Yili and Central Tianshan, and the microcontinents (e.g., Erguna and Xing'an) within northeastern China, respectively (e.g., Filippova et al. 2001; Khain et al. 2003; Windley et al. 2007; Wilhem et al. 2012; Eizenhöfer and Zhao 2018; Han and Zhao 2018; Xiao et al. 2018; Zhou et al. 2018). The Chara shear zone has been widely considered to represent the suture between the peri-Siberian and Junggar-Kazakhstan-Tianshan orogenic systems in northeastern Kazakhstan (Buslov et al. 2001, 2004; Volkova et al. 2011; Safonova et al. 2012; Safonova 2014). This zone merges with the Irtysh shear zone in northwestern China, separating Chinese Altai (i.e., part of the peri-Siberian orogenic system) to the north and West/East Junggar to the south (Li et al. 2017 and references therein; fig. 1).

Chinese Altai refers to the segment of the Altai Orogen in China (fig. 1 inset), consisting predominantly of variably metamorphosed Paleozoic sedimentary-volcanic rocks and granitoids (e.g., BGMRX 1978; Windley et al. 2002; Wang et al. 2006, 2009*a*; Long et al. 2007; Sun et al. 2008; Xiao et al. 2009; Cai et al. 2011). This segment can be subdivided into four fault-bounded tectonic domains that extend in a broadly northwest-to-southeast orientation (Long et al. 2010; Cai et al. 2012; Li et al. 2015*a*, 2015*b*, 2016*a*, 2016*b*, 2017). The Northern Altai domain represents the northernmost tectonic unit of Chinese Altai and is dominated by the Late Devonian to early Carboniferous metasedimentary sequences (Windley et al. 2002; Li et al. 2017; fig. 1). To the south, the Central Altai domain is mainly composed of early Paleozoic metasedimentary sequences, including the Habahe and Kulumuti Groups, which were suggested to be originally deposited in a continental arc–related basin surrounding western Mongolia (Long et al. 2007, 2008, 2010, 2012*b*; Jiang et al. 2011; Wang et al. 2014*b*). Most of this domain was intruded by middle-late Paleozoic granitoids (fig. 1) and, to a much lesser extent, mafic-ultramafic plutonic rocks (Wang et al. 2006, 2009*a*; Yuan et al. 2007; Sun et al. 2009*b*; Cai et al. 2010, 2011, 2012; Y. Tong et al. 2014*b*). Farther southward, the Qiongkuer domain is dominated by the Early Devonian Kangbutiebao and Middle Devonian Aletai Formations, comprising predominantly of greenschist to amphibolite facies metavolcanic/sedimentary rocks (Windley et al. 2002; Chai et al. 2009; Cai et al. 2012). The southernmost tectonic domain (i.e., the Irtysh shear zone) is represented by the Irtysh Complex, which mainly crops out west of Fuyun County and

consists of gneisses, schists, migmatites, amphibolites, and lesser quartzites and cherts (BGMRX 1978; Qu and Zhang 1991; Briggs et al. 2007; Li et al. 2015*a*, 2017). This complex underwent sinistral shear deformation in the late Paleozoic and was unconformably overlain by undeformed Permian strata (BGMRX 1978; Windley et al. 2002).

To the south, the Junggar terrane is separated from the Altai Orogen by the Irtysh fault (fig. 1) and can be subdivided into West/East Junggar and the Junggar basin (Zhang et al. 2009 and references therein). The Junggar basin is covered by ca. 10-km-thick continental sedimentary sequences with depositional ages up to Permian (Coleman 1989; Xiao et al. 2008). The basement of this basin was interpreted to be Precambrian in origin (e.g., Charvet et al. 2007; Xu et al. 2015) or to represent trapped Paleozoic oceanic crust (e.g., Xiao et al. 2008; Han and Zhao 2018) or continuations of the adjacent Altai tectonic units (Li et al. 2000 and references therein). West Junggar is in fault contact with the Yili block (not shown) to the south. In a southward direction, West Junggar successively consists of the Devonian to Carboniferous Zharma-Saur arc (fig. 1), the Cambrian to Ordovician Honguleleng ophiolite belt, the Cambrian to Silurian Boshchekul-Chingiz arc, and the Paleozoic accretionary complex, with intrusion of Devonian to Carboniferous magmatic rocks (Chen et al. 2010; Choulet et al. 2012 and references therein; Shen et al. 2012, 2015; Li et al. 2017). East Junggar consists of the Dulate arc in the north, the Yemaquan arc in the south, and the Armantai ophiolite belt in between (Zhang et al. 2008, 2009; Xiao et al. 2009; Su et al. 2012). Both arcs are dominated by Devonian to Carboniferous sedimentary and volcanic rocks (Xiao et al. 2009; Zhang et al. 2009; Li et al. 2017 and references therein), while additional minor Ordovician metasedimentary/volcanic rocks crop out in the Yemaquan arc as well (Long et al. 2012*a*).

Sampling and Petrography

Twenty-two amphibolites were collected within the Irtysh Complex. They occur as either lenticular blocks or intercalated slivers within the paraschists/gneisses (fig. 2). Samples C15-23 to C15-27 were collected from the northern domain of this complex (fig. 2), and they are characterized by porphyroblastic textures (fig. 3*a*). The porphyroblasts are exclusively garnet, containing lots of amphibole inclusions. The

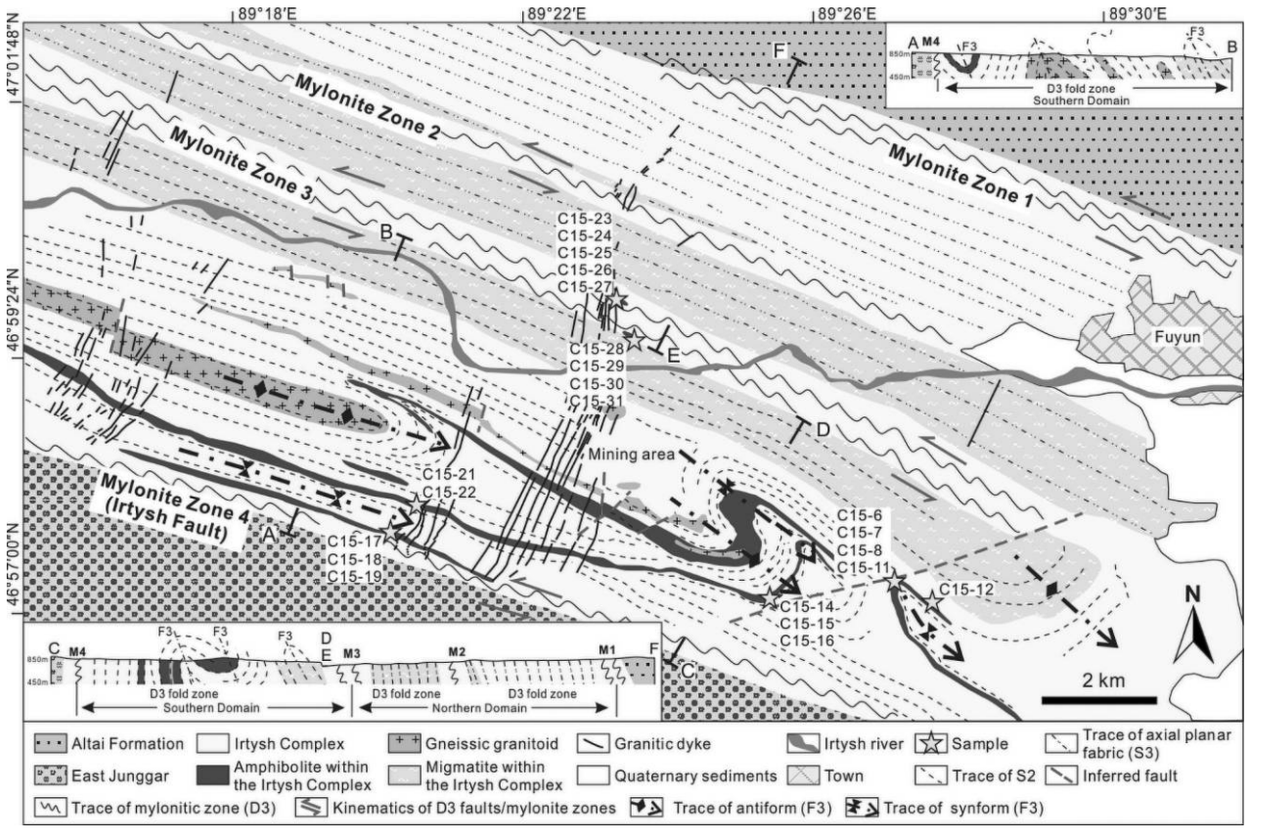

Figure 2. Geological and structural map of the Irtysh shear zone and surrounding units in the Fuyun area (modified after Li et al. 2017). M1–4 refers to mylonite zones 1–4. A color version of this figure is available online.

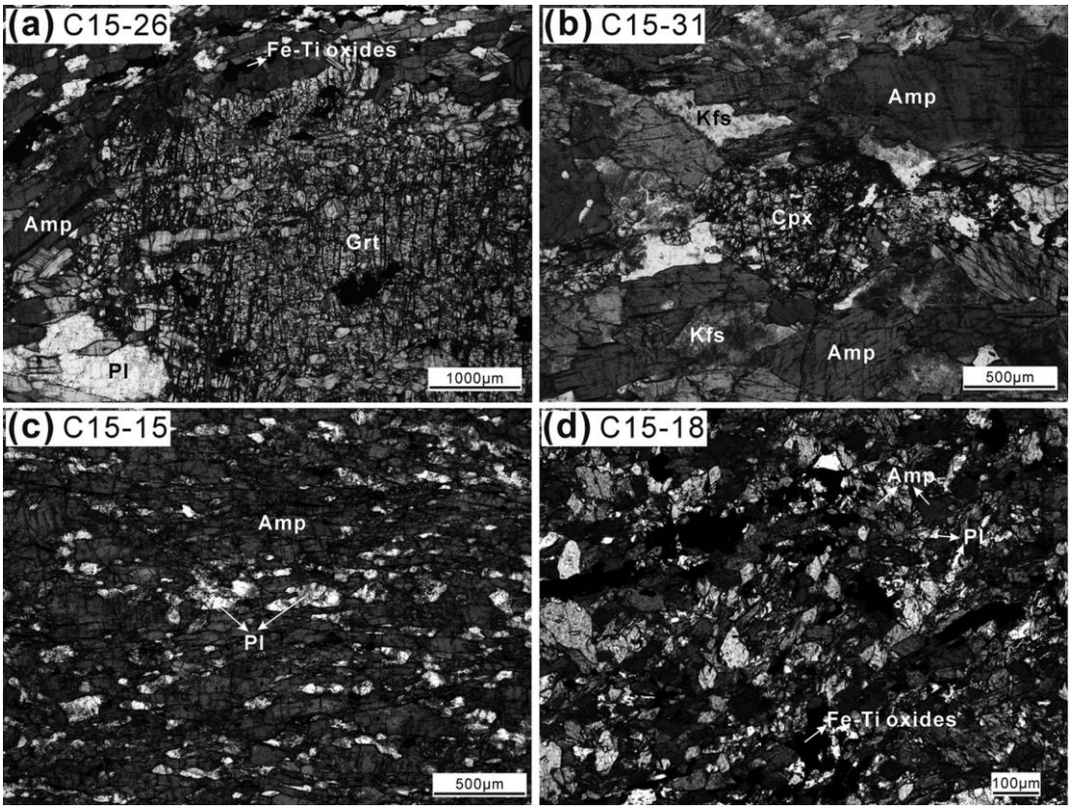

Figure 3. Petrography of representative amphibolites from Irtysh Complex in Chinese Altai. *a*, Strongly deformed garnet amphibolite that shows a porphyroblastic texture. The porphyroblasts are garnet (Grt) that contains lots of amphibole (Amp) inclusions, while the matrix has a mineral assemblage mainly of Amp, plagioclase (Pl), and minor Fe-Ti oxides. *b*, Amphibolite that comprises predominantly Amp, K-feldspar (Kfs), and, to a much lesser extent, clinopyroxene (Cpx). *c*, Strongly deformed amphibolite that consists mainly of Amp and Pl, with minor Fe-Ti oxides. *d*, Amphibolite with mineral assemblage similar to that in *c*. All these photomicrographs were obtained under plane-polarized light. A color version of this figure is available online.

matrix of these samples is composed predominantly of brown amphibole, plagioclase, and minor Fe-Ti oxides. Samples C15-28 to C15-31 were collected from the same domain, but they are devoid of porphyroblasts, consisting mainly of greenish amphibole, K-feldspar, and, to a much lesser extent, clinopyroxene (fig. 3*b*). Other samples (C15-6–8, 11–12, 14–19, and 21–22) were collected from the southern domain of the Irtysh Complex (fig. 2). They have finer-grained textures than the clinopyroxene-bearing ones and have mineral assemblages dominated by greenish amphibole and plagioclase, with minor quartz and Fe-Ti oxides (fig. 3*c*, 3*d*).

Analytical Methods

Cathodoluminescence Imaging and Zircon U-Pb Dating. Zircons were first mounted in epoxy resin and then polished down to about half their thickness. Cathodoluminescence images were obtained at the State Key Laboratory of Isotope Geochemistry (SKLIG), Guangzhou Institute of Geochemistry (GIG), Chinese Academy of Sciences (CAS).

In situ zircon dating was carried out on the Cameca IMS 1280 SIMS at the same institute, according to the procedures that were described by Li et al. (2009). The ion beam is ellipsoidal, with a size of $20 \times 30\ \mu m^2$. Standard zircon Plešovice was used to correct the U-Th-Pb isotopic ratios and absolute abundance of our analyses. All the analyses were monitored by standard zircon Qinghu. Common-Pb correction was performed with nonradiogenic ^{204}Pb. Data reduction was performed with Isoplot/Ex, version 3 (Ludwig 2003). The U-Pb dating results are presented in table S1 (tables S1–S5 are available online).

Whole-Rock Elemental and Nd Isotope Analyses. Whole-rock major-element compositions were obtained with X-ray fluorescence spectrometry (Rigaku 100e) on fused glass beads at SKLIG, GIG, CAS. For detailed analytical procedures, refer to Li et al. (2006). The analytical accuracies are estimated to be between

1% and 5%. Trace elements were measured on a Quadrupole ICP-MS at the State Key Laboratory of Ore Deposit Geochemistry, Institute of Geochemistry, CAS, Guiyang, according to the analytical method of Qi et al. (2000). About 50 mg of powder for each sample was digested in a mixture of 1 mL HF and 0.5 mL HNO_3 within closed beakers in high-pressure bombs. External calibration was conducted with a standard solution that contained the single element Rh. Standards OU-1 and AMH-1 were used as reference materials. The analytical accuracies are estimated at better than 5% for elements with concentrations of more than 200 ppm and 5%–10% for those at less than 200 ppm. The whole-rock major- and trace-element compositions are presented in table S2.

High-precision whole-rock Nd isotopic compositions were analyzed at Nanjing FocuMS Technology, with procedures similar to those reported by Li et al. (2006). Rock powders were first decomposed by high-pressure polytetrafluoroethylene bombs. Then, rare earth elements (REEs) were separated from the digesting solution by cation columns. Nd fractions were further purified by columns with LN Spec–coated Teflon powder. The Nd isotopic compositions were finally measured on a Nu Plasma II multicollector ICP-MS. The measured Nd isotopic compositions were corrected for mass fractionation by normalizing to $^{146}Nd/^{144}Nd = 0.7219$. International isotopic standard JNdi-1 was periodically analyzed to correct instrumental drift. The USGS geochemical reference materials BCR-2, BHVO-2, AVG-2, and RGM-2 were treated as quality controls. The decay constant of ^{147}Sm ($\lambda = 6.54 \times 10^{-12}$/y; Lugmair and Marti 1977) and chondritic Sm-Nd isotopic values ($^{143}Nd/^{144}Nd(0) = 0.512630$ and $^{147}Sm/^{144}Nd(0)_{CHUR} = 0.1960$ [CHUR = chondrite uniform reservoir]; Bouvier et al. 2008) were applied to calculate initial $^{143}Nd/^{144}Nd(t)$ ratios and $\varepsilon_{Nd}(t)$ values. The Sm-Nd isotopic compositions are presented in table S3.

Mineral Chemistry. Mineral compositions were analyzed on a JEOL JXA-8100 electron microprobe at SKLIG, GIG, CAS. The accelerating voltage, beam current, beam diameter, and counting time were 15 kV, 20 nA, 1–2 μm, and 10 s, respectively. The ZAF correction procedure was applied for data reduction, with the analytical uncertainty generally less than 2%. The mineral compositions are presented in table S4.

Results

Zircon U-Pb Ages. Zircons from sample C15-23 (garnet amphibolite) are subrounded to rounded and yield length/width ratios of ca. 1.0–1.5. They are generally characterized by low Th (13–113 ppm), U (183–345 ppm), and Pb (9–18 ppm) contents as well as depressed Th/U ratios of 0.06–0.33 (table S1). Importantly, zircons from this sample yield fir-tree zoning patterns (fig. 4), in contrast to those of magmatic origin. The above suggests that these zircons are metamorphic in origin. Twenty representative grains were analyzed, and they show quite homogeneous and concordant ages (fig. 4), giving a weighted mean $^{206}Pb/^{238}U$ age of 283.6 ± 1.9 Ma (MSWD = 0.26).

Whole-Rock Elemental and Nd Isotopic Compositions. Three types of amphibolites can be classified on the basis of whole-rock geochemistry. Their initial Nd isotopic compositions were calculated back to ca. 284 Ma, which represents a minimum protolith age based on the metamorphic zircon age (283.6 ± 1.9 Ma; fig. 4).

Type I. Most samples (i.e., C15-6–8, 11, 12, 17–19, and 21–27) belong to this type; of these, C15-23 was crushed for zircon separation. They have relatively large variations in SiO_2 (44.5–50.1 wt%), TiO_2 (1.48–3.44 wt%), Al_2O_3 (11.9–15.4 wt%), $Fe_2O_3^T$ (11.0–19.0 wt%), and MgO (5.92–9.90 wt%) contents, with relatively low Mg# (100 × MgO/(MgO+FeO^T), molar ratios) values of 44.1–54.1 (table S2). Samples from this group are characterized by low Nb/Y ratios of 0.05–0.12 and high FeO^T/MgO ratios of 1.51–2.26 (fig. 5), indicating tholeiitic geochemical affinity. These rocks mostly show REE patterns parallel to those of normal mid-ocean ridge basalt (N-MORB; fig. 6*a*), with $(La/Yb)_N$ (where N represents chondrite-normalized values) ratios, δEu ($2Eu_N/$

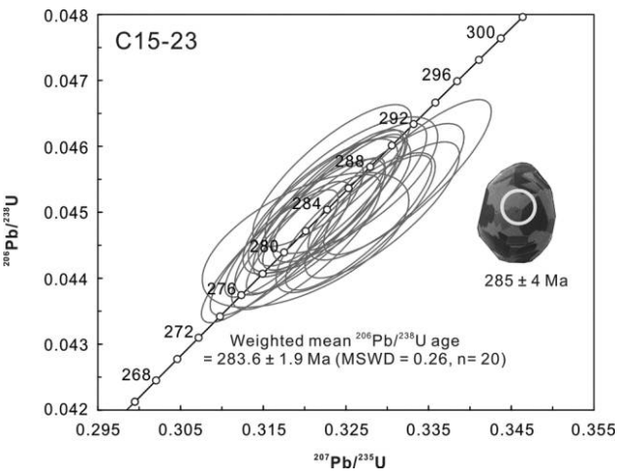

Figure 4. U-Pb concordia diagram for zircons from the garnet amphibolite C15-23. A cathodoluminescence image and a $^{206}Pb/^{238}U$ age of a representative zircon grain are shown. A color version of this figure is available online.

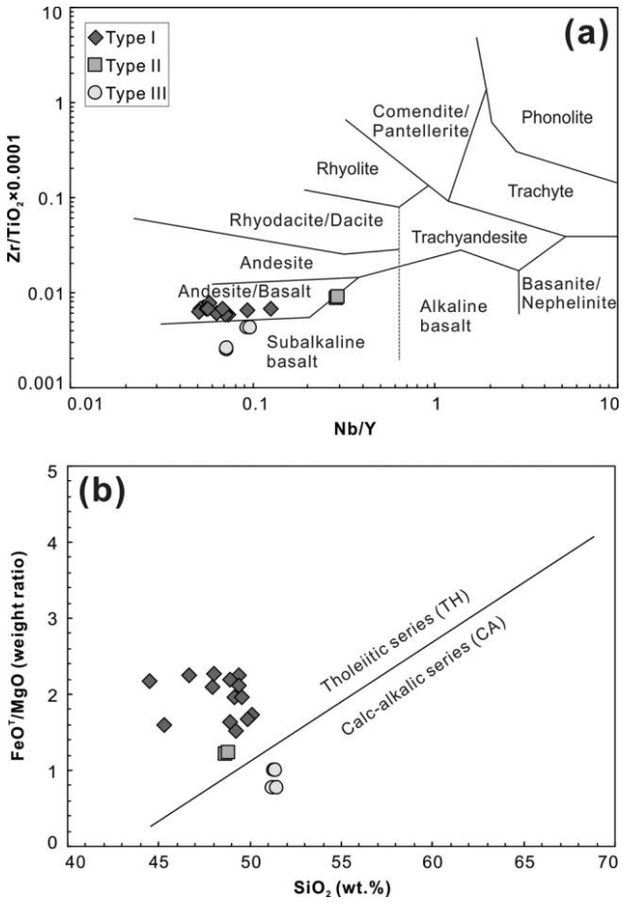

Figure 5. Nb/Y-versus-Zr/TiO_2 × 0.0001 (*a*; after Winchester and Floyd 1977) and SiO_2-versus-FeO^T/MgO (*b*) diagrams showing geochemical variations of the amphibolites from the Irtysh Complex, Chinese Altai. The line separating the tholeiitic and calc-alkaline series is after Miyashiro (1974). A color version of this figure is available online.

($Sm_N + Gd_N$)), and δCe ($2Ce_N/(La_N + Pr_N)$) varying from 0.62 to 0.82, from 0.84 to 0.94, and from 1.03 to 1.07, respectively. Samples C15-21 and C15-22 are characterized by lower heavy REE (HREE) contents and accordingly possess higher $(La/Yb)_N$ ratios of 0.92–1.15. These two samples yield insignificant Eu anomalies (δEu = 0.99–1.07) and weakly positive Ce anomalies (δCe = 1.05–1.07). No samples from this group show Nb-Ta troughs in the primitive mantle–normalized trace-element diagram (fig. 6*b*). Eight representative samples were analyzed for Nd isotopic compositions (table S3; fig. 7). They have $^{147}Sm/^{144}Nd$ ratios of 0.2051–0.2251, with $f_{Sm/Nd}$ varying from 0.05 to 0.15. The calculated $^{143}Nd/^{144}Nd$(284 Ma) and ε_{Nd}(284 Ma) are 0.512621–0.512701 and 6.9–8.5, respectively.

Type II. Only samples C15-14 and C15-15 are classified into this type. They possess nearly identical SiO_2 (48.7–48.8 wt%), TiO_2 (1.50–1.56 wt%), Al_2O_3 (15.8–15.9 wt%), $Fe_2O_3^T$ (10.8–11.0 wt%), and MgO (7.91–8.15 wt%) contents (table S2). These two samples yield higher Mg# values (59.1–59.4) and Nb/Y ratios (ca. 0.29) than their type I counterparts (fig. 5*a*). The high FeO^T/MgO ratios (1.22–1.23) suggest that type II samples also belong to the tholeiitic series (fig. 5*b*). As shown in figure 6*c*, 6*d*, samples C15-14 and C15-15 are characterized by light-REE (LREE) enrichment ($(La/Yb)_N$ = 1.90–1.94), and their REEs and other trace-element contents are comparable to those of enriched MORB (E-MORB). The Ce and Eu anomalies are negligible, with δCe of 1.02–1.03 and δEu of 1.00–1.05. In comparison with type I amphibolites, samples C15-14 and C15-15 show lower $^{147}Sm/^{144}Nd$ ratios (0.1841–0.1849) and $f_{Sm/Nd}$ (−0.06). The calculated $^{143}Nd/^{144}Nd$(284 Ma) and ε_{Nd}(284 Ma) are 0.512596–0.512598 and 6.5 (table S3; fig. 7), respectively.

Type III. Four samples (C15-28 to C15-31) are included in this type. They have slightly higher SiO_2 (51.2–51.4 wt%) but lower TiO_2 (0.32–0.42 wt%), Al_2O_3 (10.1–11.3 wt%), and $Fe_2O_3^T$ (10.6–11.3 wt%) contents than the other two types (table S2). Type III samples show diagnostically high MgO contents (10.1–12.6 wt%), with Mg# values varying from 64.1 to 70.0. In addition, they are characterized by coherently high K_2O (2.78–3.51 wt%) and low Na_2O (1.27–1.76 wt%) contents and therefore yield high K_2O/Na_2O ratios of 1.94–2.42. In contrast to the other two types, the lower FeO^T/MgO ratios of type III samples suggest their calc-alkaline geochemical affinity (fig. 5*b*). In line with their high Mg# values, all type III samples possess high Cr (407–659 ppm) and Ni (105–156 ppm) contents. They are characterized by quite low REE contents (∑REEs = 18.5–32.5 ppm), showing varying degrees of REE differentiation ($(La/Yb)_N$ = 1.56–3.12) as well as insignificant Ce and Eu anomalies (δCe = 0.92–0.95, δEu = 0.98–0.99; fig. 6*e*). All these samples display obvious depletion in high-field-strength elements (HFSEs; e.g., Nb, Zr, Hf, and Ti; fig. 6*f*). Two representative samples (C15-28 and C15-29) were analyzed for Nd isotopic composition. They yield a homogeneous $^{147}Sm/^{144}Nd$ ratio of 0.2073–0.2112, $f_{Sm/Nd}$ of 0.06–0.08, $^{143}Nd/^{144}Nd$ (284 Ma) of 0.512582–0.512585, and ε_{Nd}(284 Ma) of 6.2 (table S3; fig. 7).

Mineral Compositions. *Amphibole.* Amphiboles occur as the dominant mineral both within the matrix and within the garnet porphyroblasts of sample C15-25 (i.e., type I). Those in the former yield high CaO concentrations (9.40–10.1 wt%). They have (Ca + Na) and Na in the B site varying from 1.70 to 1.79 atoms per formula unit (apfu) and from 0.22 to 0.25 apfu (table S4), respectively, indicating calcic

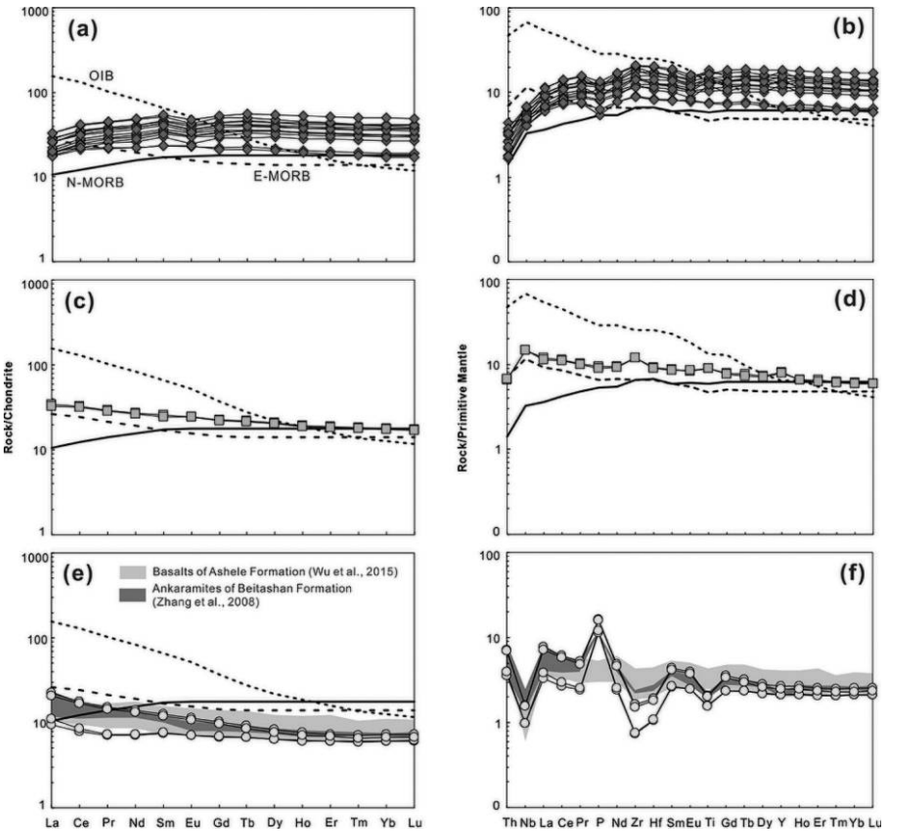

Figure 6. Trace-element compositions of the amphibolites from the Irtysh Complex, Chinese Altai. Data for the chondrite and primitive mantle are from Sun and McDonough (1989). Data for basalts of the Ashele Formation and ankaramites of the Beitashan Formation are after Wu et al. (2015) and Zhang et al. (2008), respectively. The symbols are as in figure 5. OIB = ocean island basalt; N-MORB = normal mid-ocean ridge basalt; E-MORB = enriched MORB. A color version of this figure is available online.

geochemical affinity (Leake et al. 1997). These amphiboles possess relatively high $Mg/(Mg + Fe^{2+})$ ratios of 0.63–0.66, with (Na + K) in the A site ranging from 0.29 to 0.35 apfu and Si in the T site from 6.29 to 6.45 apfu, and accordingly they can be further classified as tschermakite (fig. S1, available online) on the basis of the nomenclature scheme proposed by Leake et al. (1997). In contrast, amphiboles within the garnet porphyroblasts yield much lower CaO contents (0.42–0.99 wt%). They are characterized by low (Ca + Na) but high ($Mg + Fe^{2+}$ + Mn + Li) in the B site (0.10–0.22 and >1.78 apfu, respectively), therefore belonging to the Mg-Fe-Mn-Li group (Leake et al. 1997). The high Si (7.64–7.81 apfu) in the T site and intermediate $Mg/(Mg + Fe^{2+})$ ratios (0.58–0.60) further suggest that these amphiboles are cummingtonite (Leake et al. 1997; fig. S1).

Amphiboles from each of the other seven representative samples (i.e., C15-6, 12, 19, and 22 of type I amphibolites, C15-16 of type II, and C15-28 and 31 of type III) have quite homogeneous compositions, but they show certain differences among individual samples (fig. S1). All these amphiboles possess high CaO concentrations (9.40–12.0 wt%; table S4). Their (Ca + Na) and Na in the B site range from 1.82 to 1.96 apfu and from 0.05 to 0.18 apfu, respectively, suggesting calcic geochemical affinity (Leake et al. 1997). As shown in figure S1, these amphiboles show relatively large variations of Si in the T site (6.37–7.06 apfu) and $Mg/(Mg + Fe^{2+})$ ratios (0.49–0.76), compositionally falling in the tschermakite and magnesiohornblende fields.

Feldspar. Plagioclases from six representative amphibolites were analyzed (table S4). They show homogeneous compositions within each sample but yield slight differences among individual samples. The X_{An} (Ca/(Ca + Na + K), molar ratios) values of these plagioclases range from 0.21 to 0.48, suggesting that these grains are oligoclase or andesine. K-feldspars from samples C15-28 and C15-31 have similar compositions and, they have X_{Ab} values (Na/(Ca + Na + K)), molar ratios) varying from 0.12 to

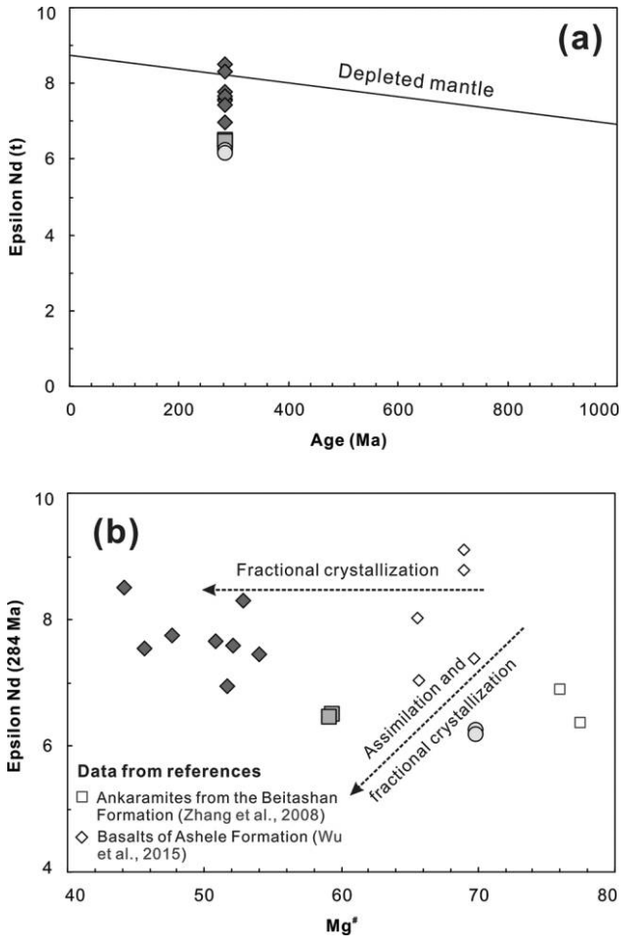

Figure 7. Nd isotope compositions of the amphibolites from Irtysh Complex, Chinese Altai. The symbols and data sources are as in figure 5. A color version of this figure is available online.

0.18 and X_{Or} values (K/(Ca + Na + K), molar ratios) from 0.82 to 0.88.

Discussion

Effects of Metamorphism and Crustal Contamination. Petrographic observation suggests that the investigated samples underwent amphibolite facies metamorphism (fig. 3). Evaluation of elemental mobility during the metamorphism is required before applying whole-rock geochemistry to discuss their source nature and petrogenesis. Zirconium (Zr) is one of the least mobile elements during metamorphism up to amphibolite facies (Polat and Hofmann 2003; Polat et al. 2003) and has been widely applied to evaluate the effect of metamorphism on other elements (e.g., Floyd et al. 1996; Chen et al. 2018). As shown in figure 8*a*–8*e*, the REEs (e.g., La, Sm, and Nd) and HFSEs (e.g., Nb and Hf) of type I amphibolites are well correlated with Zr in binary plots. Moreover, these samples all yield coherent REE patterns and insignificant Ce anomalies (fig. 6*a*). Such geochemical features imply little modification of REEs and HFSEs during the amphibolite facies metamorphism, and, accordingly, these elements can be used to investigate the origin of type I amphibolites. In contrast, large-ion lithophile elements (LILEs; e.g., Rb and U; fig. 8*f*), as well as Na_2O, K_2O and CaO (not shown), show poor correlations with Zr, suggesting their strong mobility. Since type II and III amphibolites underwent a degree of metamorphism similar to that for type I, as evidenced by the comparable mineral assemblages and calculated pressure-temperature conditions (figs. 3, 9; table S4), the above-mentioned immobile elements are also applicable to these two groups of samples.

When mantle-derived mafic melts intrude into the crust or erupt on the Earth's surface, their geochemical compositions can be variously modified as a result of different degrees of crustal contamination (e.g., DePaolo 1981; Wilson 1989). Since thorium (Th) is enriched while niobium (Nb) is depleted in the continental crust (Rudnick and Gao 2003), the lack of Th enrichment and Nb depletion in type I and II amphibolites ($(Nb/Th)_{PM}$ = 1.13–2.72 and 2.16–2.24, respectively, where PM refers to primitive mantle–normalized values; table S2) argues against significant crustal contamination during the formation of the protoliths. This is further supported by their depleted Nd isotopic compositions (ε_{Nd}(284 Ma) = 6.5–8.5; table S3; fig. 7*a*) and the absence of positive correlations between ε_{Nd}(284 Ma) and Mg# values (fig. 7*b*). Type III amphibolites possess higher Th and much lower Nb concentrations, showing obvious Nb depletion ($(Nb/Th)_{PM}$ = 0.22–0.28). Such a geochemical signature might be attributed to substantial assimilation of continental crust during the formation of the protoliths. However, we note that, in contrast to the former two types (Mg# = 44.1–59.4; ε_{Nd}(284 Ma) = 6.5–8.5; tables S2, S3), type III amphibolites possess more primitive major-element compositions (Mg# = 64.1–69.9) and similar Nd isotopic compositions (ε_{Nd}(284 Ma) = 6.2; fig. 7*b*). This suggests that assimilation of continental crust played an insignificant role in forming the protoliths of type III amphibolites, because crustal contamination would yield enriched Nd isotopic compositions and lower the Mg# values. In summary, the distinct geochemical compositions for these three types are more likely to be related to their unique petrogenetic processes and/or to reflect differences in their mantle sources.

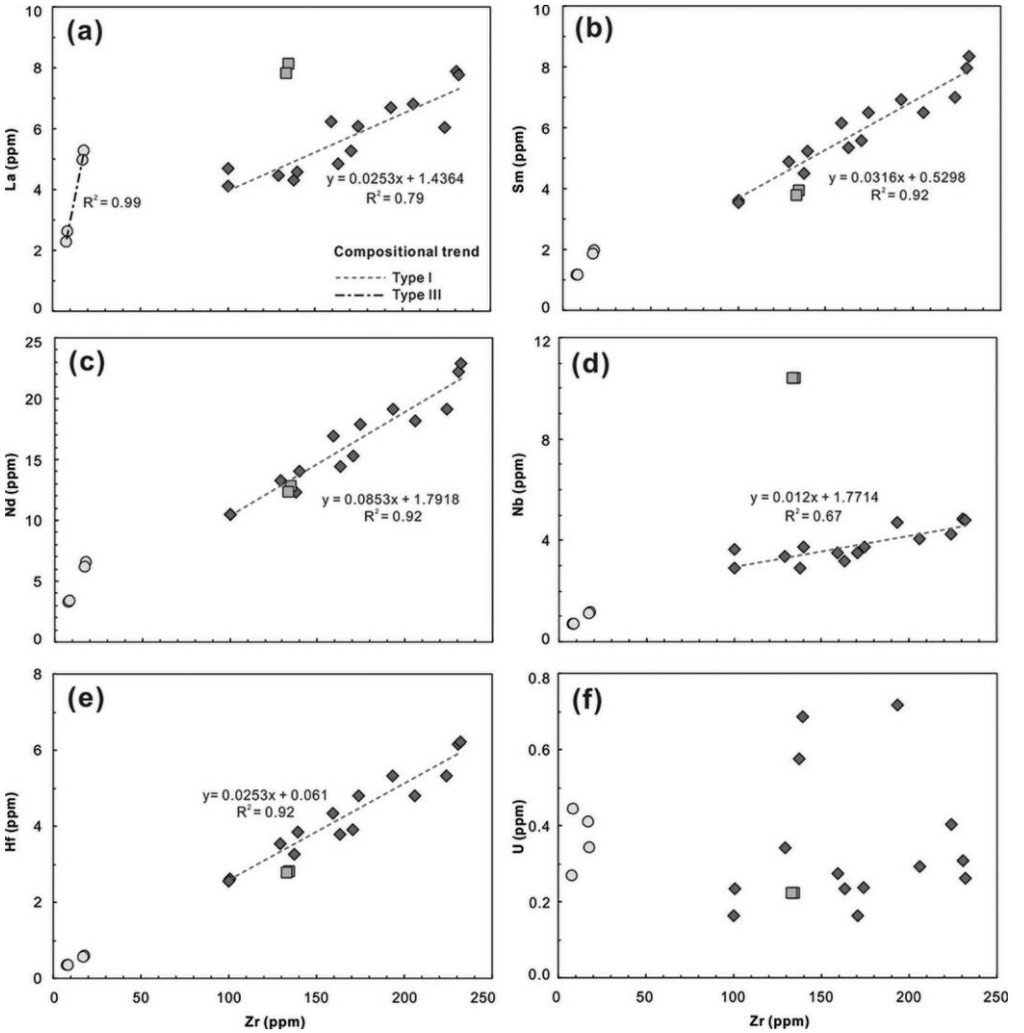

Figure 8. Binary plots showing compositional variation of the amphibolites from the Irtysh Complex, Chinese Altai. The symbols are as in figure 5. A color version of this figure is available online.

Protolith Nature of the Amphibolites. *Type I Amphibolites.* Type I amphibolites are characterized by relatively low Mg# values and Ni and Cr concentrations (table S2), suggesting that their protoliths underwent fractionation of olivine and/or pyroxene. The minor negative Eu anomalies (fig. 6*a*) further imply that plagioclase fractionation possibly also played a role.

All type I amphibolites show REE patterns (fig. 6*a*) and trace-element ratios (e.g., Zr/Y and Ti/V ratios; table S2) comparable to those of N-MORB (Sun and McDonough 1989), suggesting that the protoliths of these rocks were likely sourced from a MORB-type asthenospheric mantle. The low Th/Yb, Nb/Yb, Ba/Th, and Th/Nb ratios (fig. 10), as well as the depleted Nd isotopic compositions (fig. 7), further imply that subduction-related components were absent in their mantle source. In addition, type I amphibolites are characterized by depletion of LREEs and negligible differentiation of HREEs (fig. 6*a*), giving low $(La/Yb)_N$ ratios, mostly 0.62–0.92, and $(Gd/Yb)_N$ ratios of 1.03–1.22. This suggests that partial melting of the source mantle took place at a shallow depth above the stability field of garnet (e.g., van Westrenen et al. 2000; Sun and Liang 2013). Trace-element modeling shows that the protoliths of type I amphibolites could be produced by about 10% partial melting of depleted spinel lherzolites (McKenzie and O'Nions 1991, 1995; Aldanmaz et al. 2000; fig. 11). Such mantle source and melting degree are comparable to those of N-MORB beneath global mid-ocean ridges (e.g., Salters and Stracke 2004; Workman and Hart 2005). In the Hf/3-Th-Ta tectonic discrimination diagram (fig. 12*a*), these amphibolites exclu-

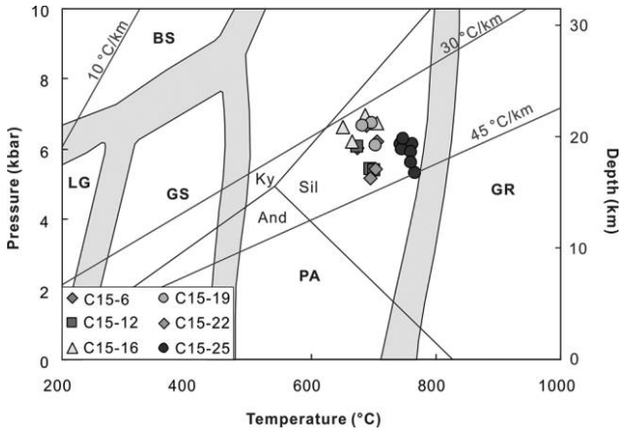

Figure 9. Metamorphic conditions of representative amphibolites from the Irtysh Complex, Chinese Altai. The subdivision of diverse metamorphic facies is based on Zheng and Chen (2017). Metamorphic facies: LG = low grade; GS = greenschist facies; BS = blueschist facies; PA = plagioclase amphibolite facies; GR = granulite facies. Minerals: Ky = kyanite; And = andalusite; Sil = sillimanite. A color version of this figure is available online.

sively plot within the N-MORB area. Taken together, our data suggest that the protoliths of type I amphibolites are likely to be N-MORB-type basalts that were generated in a mid-ocean ridge setting.

Type II Amphibolites. Type II amphibolites possess Mg# values, as well as Cr and Ni contents, slightly higher than those of type I (table S2), suggesting that the protoliths of this type underwent a lower degree of olivine and/or pyroxene fractionation. The absence of negative Eu anomalies (fig. 6*c*) further implies negligible fractionation of plagioclase, which can be reflected by the relatively high Al_2O_3 contents in these rocks.

The trace-element features of type II amphibolites are almost identical to those of E-MORB (Sun and McDonough 1989), showing enrichment of LREEs, positive Nb anomalies, relatively high Nb/Yb, Th/Yb, and La/Sm ratios, and low Ba/Th and Th/Nb ratios (figs. 6*c*, 6*d*, 10, 11). In addition, these rocks all plot within the E-MORB field in the Hf/3-Th-Ta tectonic discrimination diagram (fig. 12*a*). These data suggest that the protoliths of type II amphibolites likely represent E-MORB-type basalts. Furthermore, the low Ti/Y and Zr/Y ratios suggest their close geochemical affinity to plate margin basalts that could possibly have formed either in a mid-ocean ridge setting or in an active margin–related setting (Pearce et al. 1977; fig. 12*b*). Although some previous studies proposed that E-MORB-like basaltic rocks could be generated in an environment away from mid-ocean ridges, such as in backarc basins where spreading axes are located far from the island arcs (e.g., Taylor and Martinez 2003; Pearce and Stern 2006; Bézos et al. 2009), the basaltic rocks formed in such a setting generally show certain enrichment of LILEs and depletion of HFSEs due to minor contribution of subduction components to their mantle source, as exemplified by the basaltic rocks from the Okinawa Trough (Shinjo et al. 1999) and the Mariana Trough (Gribble et al. 1998). The absence of subduction-related trace-element signature for type II amphibolites thus rules out the formation of their protoliths in a backarc basin-related setting but supports a mid-ocean ridge environment. In the latter case, interaction between a mid-ocean ridge magma and a mantle plume (Schilling 1973; Douglass et al. 1999), low-

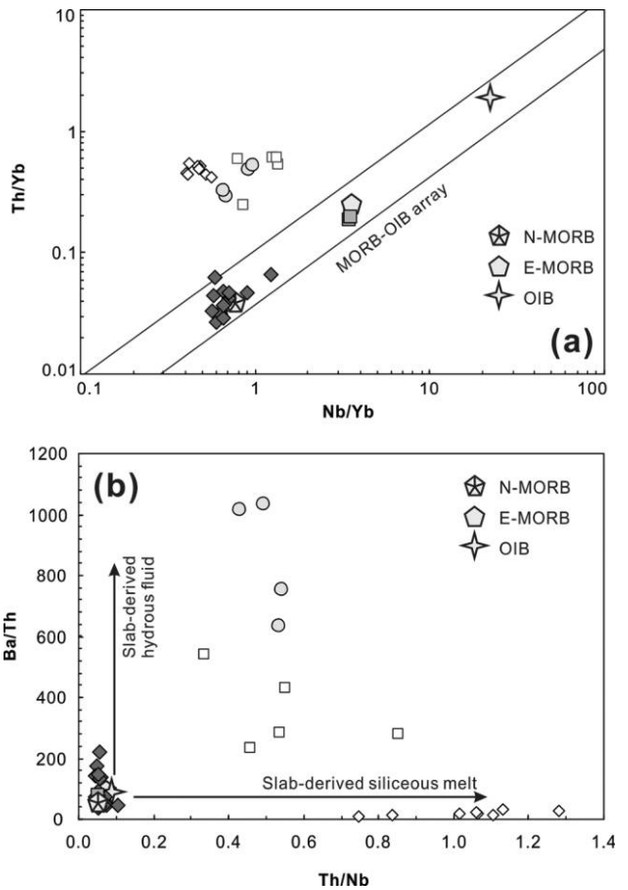

Figure 10. Nb/Yb-versus-Th/Yb (*a*; after Pearce 2008) and Th/Nb-versus-Ba/Nb (*b*) diagrams showing geochemical variations of the amphibolites from the Irtysh Complex, Chinese Altai. The symbols and data sources are as in figures 5 and 7. MORB = mid-ocean ridge basalt; N-MORB = normal MORB; E-MORB = enriched MORB; OIB = ocean island basalt. A color version of this figure is available online.

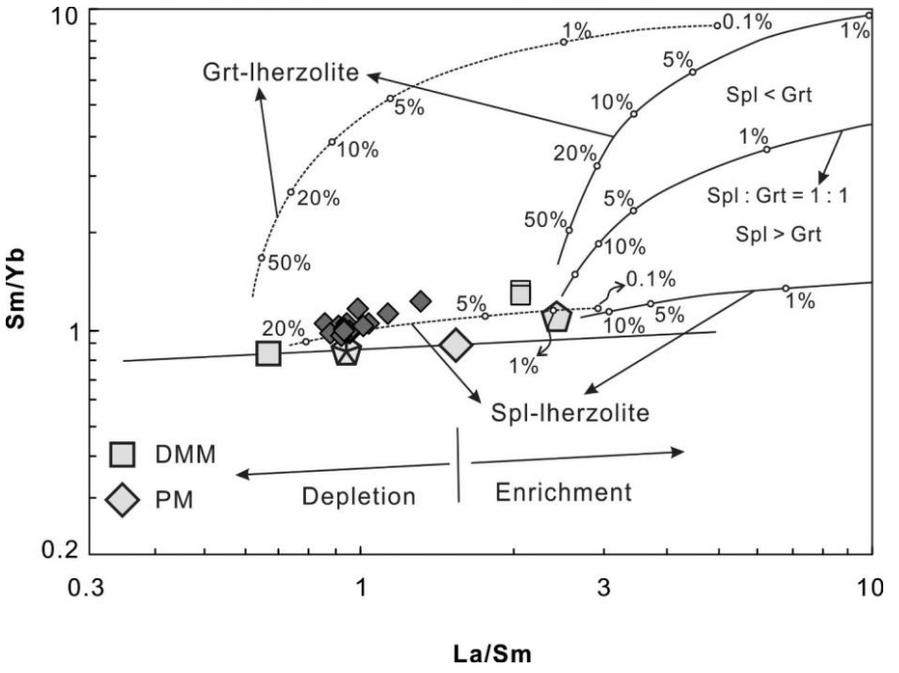

Figure 11. La/Sm-versus-Sm/Yb diagram (after Cai et al. 2010 and references therein) for the amphibolites from the Irtysh Complex, Chinese Altai. Mantle array is defined by depleted mid-ocean ridge basalt (MORB) mantle (DMM; McKenzie and O'Nions 1991) and primitive mantle (PM; Sun and McDonough 1989). Melting curves for spinel (Spl) lherzolite (Ol_{53} + Opx_{27} + Cpx_{17} + Sp_{11}) and garnet (Grt) lherzolite (Ol_{60} + Opx_{20} + Cpx_{10} + Gt_{10}) with both DMM and PM compositions are after Aldanmaz et al. (2000). Numbers along lines represent the degree of the partial melting. The symbols are as in figures 5 and 10. A color version of this figure is available online.

degree melting of mantle source similar to that of N-MORB (Choe et al. 2007; Husen et al. 2016), or partial melting of a relatively fertile mantle (Niu et al. 1999; Donnelly et al. 2004; Waters et al. 2011) could possibly account for the enriched trace-element characteristics of E-MORB-type basalts. However, the absence of ocean island basalt (OIB)–type lavas in the Irtysh shear zone, Chinese Altai, and the northern margin of East Junggar (Xiao et al. 2009 and references therein; Zhang et al. 2009) argues against plume-ridge interaction to produce the protoliths of type II amphibolites. Instead, geochemical modeling indicates that these amphibolites could have been originally produced by <5% partial melting of a depleted mantle source (i.e., spinel lherzolite; fig. 11). A higher melting degree would be expected if the

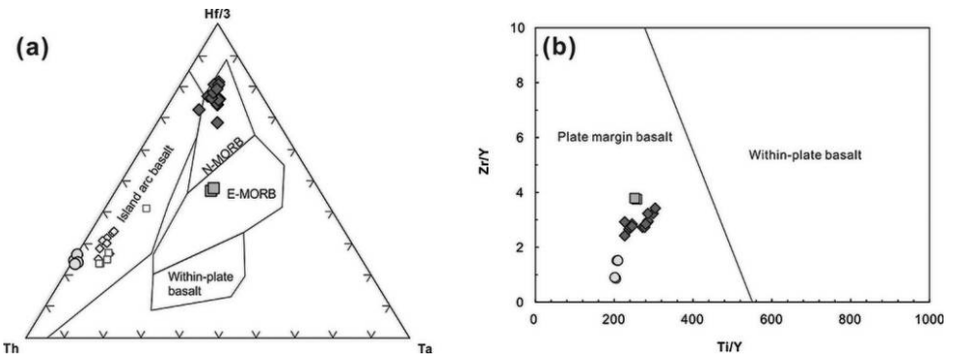

Figure 12. Hf/3-Th-Ta diagram (*a*; after Wood 1980) and Ti/Y-versus-Zr/Y diagram (*b*; after Pearce et al. 1977) showing geochemical variations of the amphibolites from the Irtysh Complex, Chinese Altai. The symbols are as in figures 5 and 7. N-MORB = normal mid-ocean ridge basalt; E-MORB = enriched MORB. A color version of this figure is available online.

mantle source was more fertile. Although uncertainties about the fertility of the mantle source, and accordingly the melting degree, exist for type II amphibolites, their ε_{Nd}(284 Ma) values (ca. 6.5), similar to those of type I (ε_{Nd}(284 Ma) = 6.9–8.5; table S3; fig. 7), support that the precursor magmas of the protolith for the two types of amphibolites both came from depleted mantle.

Type III Amphibolites. The elevated Mg# values, as well as Cr and Ni contents, for type III amphibolites (table S2) imply that their protoliths underwent negligible fractionation of olivine and/or pyroxene and therefore might be approximately in equilibrium with their mantle source. In contrast to the other two types, type III amphibolites are characterized by lower REE and HFSE contents and Sm/Yb and Zr/Yb ratios (fig. 6*e*, 6*f*), implying a more depleted mantle source that had experienced previous melt extraction.

Type III amphibolites are characterized by diagnostic HFSE depletion (e.g., Nb, Zr, Hf, and Ti; fig. 6*f*) and Nb/La ratios (0.21–0.31) much lower than those of N-MORB and E-MORB (0.93 and 1.32, respectively; Sun and McDonough 1989). In addition, these amphibolites all plot above the MORB-OIB mantle array in the Nb/Yb-versus-Th/Yb diagram (fig. 10*a*), indicating enrichment of Th. Such geochemical features suggest that their protoliths were probably generated in an arc setting with significant contribution of slab-derived components. This is consistent with their geochemical affinities to island arc basalts, as manifested in the Hf/3-Th-Ta tectonic discrimination diagram (fig. 12*a*). In general, LILEs (e.g., Ba and Pb) are mobile in hydrous fluid, while Th is more preferentially incorporated in siliceous melt (e.g., Elliott et al. 1997). The much higher Ba/Th and Th/Nb ratios for type III amphibolites (fig. 10*b*), relative to N-MORB (Ba/Th = 52.5; Th/Nb = 0.05) and E-MORB (Ba/Th = 95; Th/Nb = 0.07; Sun and McDonough 1989), therefore imply that slab-derived hydrous fluid and siliceous melt possibly both contributed to their protoliths.

Since type III amphibolites show block-in-matrix structures in the field (fig. 2), a typical feature of tectonic mélange (Festa et al. 2010; Hajná et al. 2014), and the Irtysh shear zone does not represent an arc (Xiao et al. 2009), these amphibolites or their protoliths possibly came from adjacent geological units as tectonic blocks. To the north of the Irtysh Complex, Chinese Altai underwent intense subduction-related activities in the Devonian, generating voluminous intermediate-felsic igneous rocks and subordinate mafic-ultramafic counterparts (e.g., Wang et al. 2006, 2009*a*; Yuan et al. 2007; Sun et al. 2009*b*; Cai et al. 2010, 2012; Liu et al. 2012; Chen et al. 2016*a*; Jiang et al. 2016). Among these, the ca. 388 Ma Ashele basalts in northwestern Chinese Altai have primitive major-element compositions (Mg# = 61.8–69.7), low REE concentrations, insignificant differentiation of REEs, and depletion of HFSEs (Wu et al. 2015; fig. 6*e*, 6*f*), therefore being quite similar to type III amphibolites. However, these basalts are distinctive in having positive P anomalies, which are in sharp contrast with the geochemistry of type III amphibolites (fig. 6*f*), and have more depleted Nd isotopic compositions (ε_{Nd}(284 Ma) = 7.0–9.1; fig. 7*b*; recalculation from the data by Wu et al. 2015). As such, the Ashele basalts seem unlikely to serve as the protoliths of type III amphibolites. South, but adjacent to the Irtysh shear zone, is the Dulate arc of East Junggar (fig. 1), where extensive Devonian to Carboniferous subduction-related volcanic rocks crop out (Zhang et al. 2008, 2009; Su et al. 2012). We note that the ankaramites from the middle Devonian Beitashan formation (Zhang et al. 2008), which were thought to represent immature island arc products by northward subduction of the Junggar Ocean (Zhang et al. 2008 and references therein), show both positive P anomalies and other trace-element signatures as well as whole-rock Nd isotopic compositions almost identical to those of type III amphibolites (figs. 6*e*, 6*f*, 7*b*). This implies that the protoliths of these amphibolites were possibly same as the ankaramites from the Dulate arc.

Late Paleozoic Accretionary Processes along the Southern Peri-Siberian Orogenic System. As discussed above, the protoliths of amphibolites within the Irtysh Complex are characterized by diverse origins and came from different tectonic settings, that is, a mid-ocean ridge and an island arc. Importantly, their occurrence as either lenticular blocks or intercalated slivers within the paraschists/gneisses (fig. 2) and their close spatial association with cherts, limestones, and gneissic granitoids (Briggs et al. 2007; Xiao et al. 2009 and references therein; Li et al. 2015*a*, 2017) support that the Irtysh Complex probably represents an accretionary prism. Recent detrital zircon U-Pb-Hf isotopic data revealed that the protoliths of the metasedimentary rocks from this complex were likely sourced from Chinese Altai, not East Junggar (Li et al. 2015*a*, 2017). This indicates that the Irtysh Complex was possibly built upon the southern margin of Chinese Altai, receiving sediments from the eroded products of this tectonic unit.

Paleogeographic reconstruction suggests that the Kazakhstan continent and adjacent intraoceanic arcs of the Junggar terrane were possibly located in the central part of the Paleo-Asian Ocean in the Early Devonian, dividing this giant ocean into four branches (i.e., the Ob-Zaisan, Uralian, Turkestan, and Junggar-

Balkhash Oceans; Filippova et al. 2001; Windley et al. 2007; fig. 13*a*). The voluminous Devonian arc-type igneous rocks in the Altai Orogen, including the segment in China (i.e., Chinese Altai), were attributed to northward subduction of the Ob-Zaisan Ocean along the southern margin (present coordinates) of the peri-Siberian orogenic system (fig. 13*a*; e.g., Wang et al. 2006; Yuan et al. 2007; Sun et al. 2009*b*; Cai et al. 2010, 2011, 2012; Glorie et al. 2011; Kruk et al. 2011; Liu et al. 2012; Chen et al. 2016*a*; Jiang et al. 2016). We propose that the protoliths of type I and II amphibolites probably represent the relicts scraped off from the crust of this oceanic branch when it subducted beneath the active margin of Chinese Altai (fig. 13*b*). The absence of peridotites (i.e., deeper parts of the oceanic lithosphere of the Ob-Zaisan Ocean) within the Irtysh Complex might imply a rugged topography for the oceanic plate entering the subduction zone (Hajná et al. 2014), with only the uppermost layer being plucked. Because the arc activity in East Junggar was predominantly in the Devonian to Carboniferous (Xiao et al. 2009; Zhang et al. 2009; Li et al. 2017 and references therein), the identification of Ordovician gneissic granitoids within the Irtysh Complex, which have ages and geochemistry comparable to those of Chinese Altai (Briggs et al. 2007; Cai et al. 2011), implies that some lithological units of the overriding plate were also incorporated during the subduction-accretion processes. Importantly, the youngest detrital zircon age of ca. 322 Ma for the metasedimentary units of this complex (Li et al. 2015*a*), in combination with the identification of ca. 313 Ma arc-related magmatism in Chinese Altai (Cai et al. 2012), suggests that the subduction-accretion along the southern margin of the peri-Siberian orogenic system lasted at least until the late Carboniferous (fig. 13*b*), therefore arguing against amalgamation between Chinese Altai and East Junggar in the Late Devonian, as proposed by Hong et al. (2017). After consumption of the Ob-Zaisan Ocean (<313 Ma), the accretion of East Junggar to the Altai Orogen ultimately brought the magmatic products of the Dulate arc, as represented by the protoliths of type III amphibolites, into the Irtysh Complex, possibly by tectonic mingling (fig. 13*c*). This complex therefore documents multiple lateral growth of an accretionary prism along the southern margin of the peri-Siberian orogenic system.

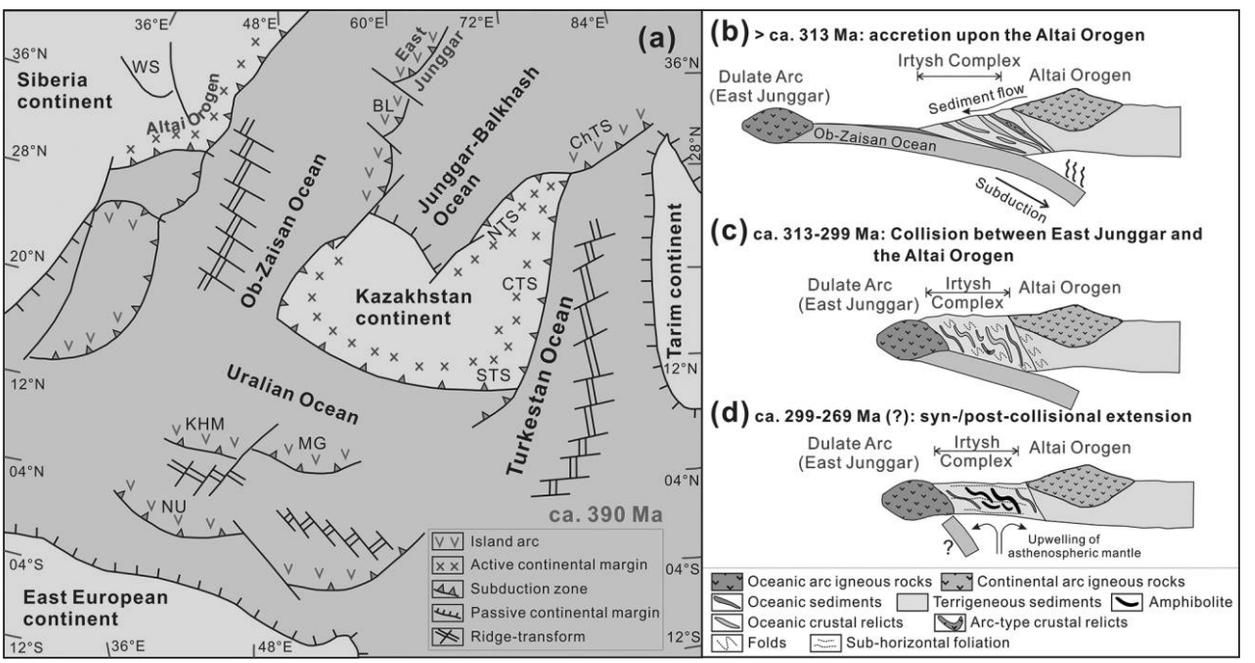

Figure 13. *a*, Paleogeographic reconstruction diagram (modified after Filippova et al. 2001 and Windley et al. 2007) showing that the Kazakhstan continent and the intraoceanic arcs of the Junggar terrane were situated in the central part of the Paleo-Asian Ocean (PAO) ca. 390 Ma. The Altai Orogen, as part of the peri-Siberia orogenic system, was under subduction of the intervening Ob-Zaisan Ocean (i.e., a branch of the PAO) between this orogenic system and the Kazakhstan-Junggar orogenic collage. BL = Barlyk arc; ChTS = Chinese Tien Shan; CTS = Central Tien Shan; KHM = Khanty-Mansi; MG = Magnitogorsk; NTS = North Tien Shan; NU = North Urals; STS = South Tien Shan; and WS = West Sayan. *b–d*, Schematic cartoons illustrating the accretionary and collisional processes between the Altai Orogen and East Junggar. A color version of this figure is available online.

Permian Metamorphism and Its Tectonic Implication. Metamorphic zircons from sample C15-23 (i.e., type I amphibolite) yield a weighted mean $^{206}Pb/^{238}U$ age of 283.6 ± 1.9 Ma (fig. 4), suggesting that amphibolite facies metamorphism took place in the early Permian. Equilibrated amphibole-plagioclase pairs from six representative amphibolites were selected to constrain the metamorphic pressure-temperature conditions through combined aluminum-in-hornblende barometry (Schmidt 1992; Anderson and Smith 1995) and a hornblende-plagioclase thermometer (Blundy and Holland 1990; Holland and Blundy 1994). The five amphibolites without garnet porphyroblasts (samples C15-6, 12, 16, 19, and 22) show relatively homogeneous metamorphic temperatures ranging from 651° to 706°C (average: 688°C) and varied metamorphic pressures of 5.18–6.95 kbar (average: 6.17; fig. 9; table S4). The garnet amphibolite (sample C15-25) yields comparable metamorphic pressures of 5.33–6.29 kbar (average: 5.92) but shows slightly higher metamorphic temperatures of 743°–766°C (average: 755°C; fig. 9; table S4). Despite the subtle differences among individual samples, the calculated pressure-temperature conditions exclusively point out that the Irtysh shear zone was under a high geothermal gradient of 30°–45°C/km (fig. 9) at ca. 284 Ma. This is consistent with the wide occurrence of coeval leucogranitic/granitic dikes and migmatites by crustal remelting and high-temperature metamorphism within the same tectonic unit (Han et al. 2006; Tong et al. 2006*a*, 2006*b*, 2014*b*; Briggs et al. 2007; Gong et al. 2007; Zhang et al. 2012; Yang et al. 2015; Hong et al. 2017; Li et al. 2017). The above data imply that the Irtysh shear zone was under an uncommon tectonic setting involving remarkably high heat flux from a deep-seated source in the early Permian.

Recently, on the basis of structural investigation, Li et al. (2015*a*, 2015*b*, 2017) proposed that the amalgamation between East Junggar and Chinese Altai in the late Paleozoic involved an initial episode of contraction and crustal thickening, which was followed by extensional tectonics, as indicated by subhorizontal foliations and orogen-parallel stretching lineations (Li et al. 2017). As discussed in "Late Paleozoic Accretionary Processes along the Southern Peri-Siberian Orogenic System," Chinese Altai was possibly still an active continental margin setting at ca. 313 Ma. Therefore, the ca. 295 Ma high-temperature metamorphism recorded by the metamorphic zircon rims from the mica schist and migmatite from the Irtysh Complex (Li et al. 2015*a*, 2017) may suggest that the orogenic thickening took place between ca. 313 and 295 Ma. Moreover, the ca. 299 Ma high-temperature and low-pressure metamorphism identified along the southern margin of Chinese Altai (Wang et al. 2014*a*) implies that the syn-/postcollisional extension, in association with high heat fluxes, might have been initiated as early as the earliest Permian. Data compilation (table S5), including the newly obtained metamorphic age in this study, shows that the high- to ultrahigh-temperature metamorphism within the Irtysh shear zone and the southern margin of Chinese Altai lasted from ca. 299 to 269 Ma (fig. 14; Chen et al. 2006*a*, 2006*b*; Wang et al. 2009*b*, 2014*a*; Z. Li et al. 2014; Tong et al. 2014*a*; P. Li et al. 2015*a*, 2017). Importantly, these metamorphic records are broadly coeval with the spatially associated mafic intrusions with an asthenospheric origin (fig. 14; Han et al. 2004; Zhang et al. 2010, 2014; Wan et al. 2013; Yang et al. 2015; Cai et al. 2016) and crust-derived felsic magmatism (i.e., leucogranitic/granitic dikes, granitic plutons, and leucosomes within migmatites; Wang et al. 2005; Han et al. 2006; Tong et al. 2006*a*, 2006*b*, 2014*b*; Briggs

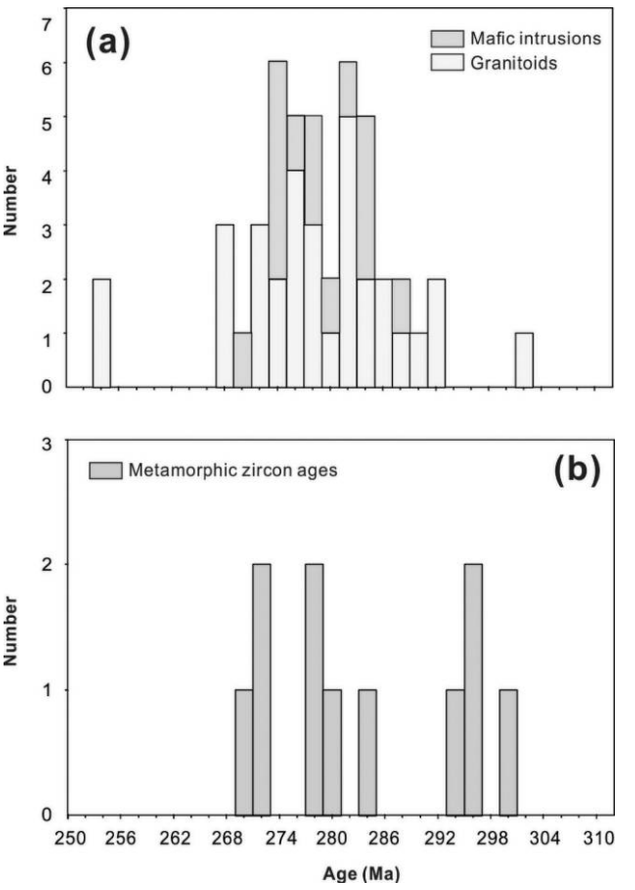

Figure 14. Age distributions of the Permian magmatic rocks and high- to ultrahigh-temperature metamorphism along the Irtysh shear zone. The data sources are summarized in table S5, available online. A color version of this figure is available online.

et al. 2007; Gong et al. 2007; Zhou et al. 2007*a*, 2007*b*, 2009; G. Sun et al. 2009*a*; M. Sun et al. 2009*b*; Gao et al. 2010; Ren et al. 2011; Li et al. 2012; Zhang et al. 2012; Yang et al. 2015; Cai et al. 2016; Hong et al. 2017). Given that $^{40}Ar/^{39}Ar$ studies suggest a major cooling event through hornblende/mica closure temperature ca. 280–270 Ma (Briggs et al. 2007; Li et al. 2017), it remains enigmatic whether the syn-/post-collisional extension lasted until ca. 269 Ma. However, the resultant elevated heat fluxes in the early Permian likely triggered high- to ultrahigh-temperature metamorphism and promoted partial melting of preexisting crust to form granitic magmatism with or without input of mantle-derived mafic melts (fig. 13*d*). These contributed significantly to the vertical differentiation and possible growth of continental crust along the Irtysh shear zone.

Conclusions

1. Three types of amphibolites are identified within the Irtysh Complex, Chinese Altai. The protoliths of type I and type II are N-MORB- and E-MORB-type basalts, respectively, which possibly represent crustal relicts of the Ob-Zaisan Ocean between the peri-Siberian and Kazakhstan-Junggar orogenic systems. In contrast, ankaramites from the Dulate arc of East Junggar or chemical equivalents possibly served as the protoliths of type III amphibolites.

2. The Irtysh Complex represents an accretionary prism built upon the southern margin of Chinese Altai, and the subduction-accretion continued until ca. 313 Ma.

3. The Chinese Altai (i.e., part of the peri-Siberian orogenic system) and East Junggar (i.e., part of the Kazakhstan-Junggar orogenic system) collided between ca. 313 and 299 Ma, followed by an episode of extension in the early Permian. In the latter process, upwelling of mantle-derived melts gave rise to high- to ultrahigh-temperature metamorphism and crustal melting.

ACKNOWLEDGMENTS

We are grateful to editor D. B. Rowley and an anonymous reviewer for their constructive comments that significantly improved the manuscript. This study was financially supported by the National Key R&D Program of China (2017YFC0601205), the Major Basic Research Project of the Ministry of Science and Technology of China (2014CB440801 and 2014CB448000), the Hong Kong Research Council (17303415 and 17302317), the National Science Foundation of China (41703032, 41622205, 41273048, and 41190075), and the Fundamental Research Funds for the Central Universities, China University of Geosciences (Wuhan; CUG170628), and, for P. Li, the Young Thousand Talents Program. The work is a contribution to the IGCP592 project by the Joint Laboratory of Chemical Geodynamics between the University of Hong Kong and Guangzhou Institute of Geochemistry, Chinese Academy of Sciences.

REFERENCES CITED

Aldanmaz, E.; Pearce, J.; Thirlwall, M.; and Mitchell, J. 2000. Petrogenetic evolution of late Cenozoic, post-collision volcanism in western Anatolia, Turkey. J. Volcanol. Geotherm. Res. 102:67–95.

Anderson, J. L., and Smith, D. R. 1995. The effects of temperature and fO_2 on the Al-in-hornblende barometer. Am. Mineral. 80:549–559.

Bézos, A.; Escrig, S.; Langmuir, C. H.; Michael, P. J.; and Asimow, P. D. 2009. Origins of chemical diversity of back-arc basin basalts: a segment-scale study of the Eastern Lau Spreading Center. J. Geophys. Res. Solid Earth 114:B06212. doi:10.1029/2008JB005924.

BGMRX (Bureau of Geology and Mineral Resources of Xinjiang Autonomous Region). 1978. Geological map and explanatory note of the Fuyun sheet, scale 1:200,000.

Blundy, J. D., and Holland, T. J. 1990. Calcic amphibole equilibria and a new amphibole-plagioclase geothermometer. Contrib. Mineral. Petrol. 104:208–224.

Bouvier, A.; Vervoort, J. D.; and Patchett, P. J. 2008. The Lu-Hf and Sm-Nd isotopic composition of CHUR: constraints from unequilibrated chondrites and implications for the bulk composition of terrestrial planets. Earth Planet. Sci. Lett. 273:48–57.

Briggs, S. M.; Yin, A.; Manning, C. E.; Chen, Z.-L.; Wang, X.-F.; and Grove, M. 2007. Late Paleozoic tectonic history of the Ertix Fault in the Chinese Altai and its implications for the development of the Central Asian Orogenic System. Geol. Soc. Am. Bull. 119:944–960.

Buslov, M. M.; Saphonova, I. Y.; Watanabe, T.; Obut, O. T.; Fujiwara, Y.; Iwata, K.; Semakov, N. N.; Sugai, Y.; Smirnova, L. V.; and Kazansky, A. Y. 2001. Evolution of the Paleo-Asian Ocean (Altai-Sayan Region, Central Asia) and collision of possible Gondwana-derived terranes with the southern marginal part of the Siberian continent. Geosci. J. 5:203–224.

Buslov, M. M.; Watanabe, T.; Fujiwara, Y.; Iwata, K.; Smirnova, L. V.; Safonova, I. Y.; Semakov, N. N.; and Kiryanova, A. P. 2004. Late Paleozoic faults of the Altai region, Central Asia: tectonic pattern and model of formation. J. Asian Earth Sci. 23:655–671.

Cai, K.; Sun, M.; Jahn, B.-m.; Xiao, W.; Long, X.; Chen, H.; Xia, X.; Chen, M.; and Wang, X. 2016. Petrogenesis of the Permian intermediate-mafic dikes in the Chinese Altai, Northwest China: implication for a postaccretion extensional scenario. J. Geol. 124:481–500.

Cai, K.; Sun, M.; Yuan, C.; Xiao, W.; Zhao, G.; Long, X.; and Wu, F. 2012. Carboniferous mantle-derived felsic intrusion in the Chinese Altai, NW China: implications for geodynamic change of the accretionary orogenic belt. Gondwana Res. 22:681–698.

Cai, K.; Sun, M.; Yuan, C.; Zhao, G.; Xiao, W.; Long, X.; and Wu, F. 2010. Geochronological and geochemical study of mafic dykes from the northwest Chinese Altai: implications for petrogenesis and tectonic evolution. Gondwana Res. 18:638–652.

———. 2011. Prolonged magmatism, juvenile nature and tectonic evolution of the Chinese Altai, NW China: evidence from zircon U-Pb and Hf isotopic study of Paleozoic granitoids. J. Asian Earth Sci. 42:949–968.

Cawood, P. A.; Kröner, A.; Collins, W. J.; Kusky, T. M.; Mooney, W. D.; and Windley, B. F. 2009. Accretionary orogens through Earth history. *In* Cawood, P. A., and Kröner, A., eds. Earth accretionary systems in space and time. Geol. Soc. Lond. Spec. Publ. 318:1–36.

Chai, F.; Mao, J.; Dong, L.; Yang, F.; Liu, F.; Geng, X.; and Zhang, Z. 2009. Geochronology of metarhyolites from the Kangbutiebao Formation in the Kelang basin, Altay Mountains, Xinjiang: implications for the tectonic evolution and metallogeny. Gondwana Res. 16:189–200.

Charvet, J.; Shu, L. S.; and Laurent-Charvet, S. 2007. Paleozoic structural and geodynamic evolution of eastern Tianshan (NW China): welding of the Tarim and Junggar plates. Episodes 30:162–186.

Chen, H. L.; Li, Z. L.; Yang, S. F.; Dong, C. W.; Xiao, W. J.; and Tainosho, Y. 2006*a*. Mineralogical and geochemical study of a newly discovered mafic granulite, northwest China: implications for tectonic evolution of the Altay Orogenic Belt. Isl. Arc 15:210–222.

Chen, H. L.; Yang, S. F.; Li, Z. L.; Yu, X.; Xiao, W. J.; Yuan, C.; Lin, X. B.; and Li, J. L. 2006*b*. Zircon SHRIMP U-Pb chronology of Fuyun basic granulite and its tectonic significance in Altaid orogenic belt. Acta Petrol. Sin. 22:1351–1358 (in Chinese with English abstract).

Chen, J.-F.; Han, B.-F.; Ji, J.-Q.; Zhang, L.; Xu, Z.; He, G.-Q.; and Wang, T. 2010. Zircon U-Pb ages and tectonic implications of Paleozoic plutons in northern West Junggar, North Xinjiang, China. Lithos 115:137–152.

Chen, M.; Sun, M.; Buslov, M. M.; Cai, K.; Jiang, Y.; Kulikova, A. V.; Zheng, J.; and Xia, X. 2018. Variable slab-mantle interaction in a nascent Neoproterozoic arc-back-arc system generating boninitic-tholeiitic lavas and magnesian andesites. Geol. Soc. Am. Bull. 130: 1562–1582.

Chen, M.; Sun, M.; Buslov, M. M.; Cai, K.; Zhao, G.; Kulikova, A. V.; and Rubanova, E. S. 2016*a*. Crustal melting and magma mixing in a continental arc setting: evidence from the Yaloman intrusive complex in the Gorny Altai terrane, Central Asian Orogenic Belt. Lithos 252:76–91.

Chen, M.; Sun, M.; Buslov, M. M.; Cai, K.; Zhao, G.; Zheng, J.; Rubanova, E. S.; and Voytishek, E. E. 2015*a*. Neoproterozoic–middle Paleozoic tectono-magmatic evolution of the Gorny Altai terrane, northwest of the Central Asian Orogenic Belt: constraints from detrital zircon U-Pb and Hf-isotope studies. Lithos 233:223–236.

Chen, M.; Sun, M.; Cai, K.; Buslov, M. M.; Zhao, G.; Jiang, Y.; Rubanova, E. S.; Kulikova, A. V.; and Voytishek, E. E. 2016*b*. The early Paleozoic tectonic evolution of the Russian Altai: implications from geochemical and detrital zircon U-Pb and Hf isotopic studies of metasedimentary complexes in the Charysh-Terekta-Ulagan-Sayan suture zone. Gondwana Res. 34:1–15.

Chen, M.; Sun, M.; Cai, K.; Buslov, M. M.; Zhao, G.; and Rubanova, E. S. 2014. Geochemical study of the Cambrian–Ordovician meta-sedimentary rocks from the northern Altai-Mongolian terrane, northwestern Central Asian Orogenic Belt: implications on the provenance and tectonic setting. J. Asian Earth Sci. 96:69–83.

Chen, M.; Sun, M.; Cai, K.; Buslov, M. M.; Zhao, G.; Rubanova, E. S.; and Voytishek, E. E. 2015*b*. Detrital zircon record of the early Paleozoic meta-sedimentary rocks in Russian Altai: implications on their provenance and the tectonic nature of the Altai-Mongolian terrane. Lithos 233:209–222.

Choe, W. H.; Lee, J. I.; Lee, M. J.; Hur, S. D.; and Jin, Y. K. 2007. Origin of E-MORB in a fossil spreading center: the Antarctic-Phoenix Ridge, Drake Passage, Antarctica. Geosci. J. 11:185–199.

Choulet, F.; Cluzel, D.; Faure, M.; Lin, W.; Wang, B.; Chen, Y.; Wu, F.; and Ji, W. 2012. New constraints on the pre-Permian continental crust growth of Central Asia (West Junggar, China) by U-Pb and Hf isotopic data from detrital zircon. Terra Nova 24:189–198.

Coleman, R. G. 1989. Continental growth of northwest China. Tectonics 8(3):621–635.

Condie, K. C. 2007. Accretionary orogens in space and time. *In* Hatcher, R. D., Jr.; Carlson, M. P.; McBride, J. H.; and Martínez Catalán, J. R., eds. 4-D framework of continental crust. Geol. Soc. Am. Mem. 200:145–158.

Condie, K. C., and Kröner, A. 2008. When did plate tectonics begin? evidence from the geologic record. *In* Condie, K. C., and Pease, V., eds. When did plate tectonics begin on planet Earth? Geol. Soc. Am. Spec. Pap. 440:281–294.

Demoux, A.; Kröner, A.; Badarch, G.; Jian, P.; Tomurhuu, D.; and Wingate, M. T. D. 2009. Zircon ages from the Baydrag Block and the Bayankhongor ophiolite zone: time constraints on late Neoproterozoic to Cambrian subduction- and accretion-related magmatism in central Mongolia. J. Geol. 117:377–397.

DePaolo, D. J. 1981. Trace element and isotopic effects of combined wallrock assimilation and fractional crystallization. Earth Planet. Sci. Lett. 53:189–202.

Dobretsov, N. L.; Berzin, N. A.; and Buslov, M. 1995. Opening and tectonic evolution of the Paleo-Asian Ocean. Int. Geol. Rev. 37:335–360.

Donnelly, K. E.; Goldstein, S. L.; Langmuir, C. H.; and Spiegelman, M. 2004. Origin of enriched ocean ridge basalts and implications for mantle dynamics. Earth Planet. Sci. Lett. 226:347–366.

Douglass, J.; Schilling, J.; and Fontignie, D. 1999. Plume-ridge interactions of the Discovery and Shona mantle plumes with the southern Mid-Atlantic Ridge (40°–55°S). J. Geophys. Res. Solid Earth 104:2941–2962.

Eizenhöfer, P. R., and Zhao, G. 2018. Solonker Suture in East Asia and its bearing on the final closure of the eastern segment of the Palaeo-Asian Ocean. Earth-Sci. Rev. 186:153–172.

Elliott, T.; Plank, T.; Zindler, A.; White, W.; and Bourdon, B. 1997. Element transport from slab to volcanic front at the Mariana arc. J. Geophys. Res. Solid Earth 102: 14,991–15,019.

Festa, A.; Pini, G. A.; Dilek, Y.; and Codegone, G. 2010. Mélanges and mélange-forming processes: a historical overview and new concepts. Int. Geol. Rev. 52:1040–1105.

Filippova, I. B.; Bush, V. A.; and Didenko, A. N. 2001. Middle Paleozoic subduction belts: the leading factor in the formation of the Central Asian fold-and-thrust belt. Russ. J. Earth Sci. 3:405–426.

Floyd, P. A.; Winchester, J. A.; Ciesielczuk, J.; Lewandowska, A.; Szczepanski, J.; and Turniak, K. 1996. Geochemistry of early Palaeozoic amphibolites from the Orlica-Śnieżnik dome, Bohemian massif: petrogenesis and palaeotectonic aspects. Int. J. Earth Sci. 85:225–238.

Gao, F. P.; Zhou, G.; Lei, X. Y.; Wang, D. S.; Chen, J. X.; Zhang, H. F.; Wu, X. B.; Liu, G. R.; and Zhao, Z. H. 2010. Early Permian granite age and geochemical characteristics in Shaerbulake of Xinjiang's Altay area and its geological significance. Geol. Bull. China 29:1281–1293 (in Chinese with English abstract).

Gao, J.-F., and Zhou, M.-F. 2013. Magma mixing in the genesis of the Kalatongke dioritic intrusion: implications for the tectonic switch from subduction to post-collision, Chinese Altay, NW China. Lithos 162–163: 236–250.

Glorie, S.; De Grave, J.; Buslov, M. M.; Zhimulev, F. I.; Izmer, A.; Vandoorne, W.; Ryabinin, A.; Van den Haute, P.; Vanhaecke, F.; and Elburg, M. 2011. Formation and Palaeozoic evolution of the Gorny-Altai–Altai-Mongolia suture zone (South Siberia): zircon U/Pb constraints on the igneous record. Gondwana Res. 20:465–484.

Gong, H. L.; Chen, Z. L.; Hu, Y. Q.; Li, L.; Lai, X. R.; Ma, Q. Y.; Li, Y. Y.; Hu, B.; and Zhang, W. G. 2007. Geochemical characteristics of acidic dikes swarms from the eastern segment of the Ertix tectonic belt, Altai orogeny and its geological implications. Acta Petrol. Sin. 23:889–899 (in Chinese with English abstract).

Gribble, R. F.; Stern, R. J.; Newman, S.; Bloomer, S. H.; and O'Hearn, T. 1998. Chemical and isotopic composition of lavas from the northern Mariana Trough: implications for magmagenesis in back-arc basins. J. Petrol. 39:125–154.

Hajná, J.; Žák, J.; and Kachlik, V. 2014. Growth of accretionary wedges and pulsed ophiolitic mélange formation by successive subduction of trench-parallel volcanic elevations. Terra Nova 26:322–329.

Han, B. F.; Ji, J. Q.; Song, B.; Chen, L. H.; and Li, Z. H. 2004. SHRIMP U-Pb zircon age of the mafic-ultramafic rocks and geological significance in Karatungk and Huangshan, Xinjiang. Chin. Sci. Bull. 49:2324–2328 (in Chinese).

Han, B. F.; Ji, J. Q.; Song, B.; Chen, L. H.; and Zhang, L. 2006. Late Paleozoic vertical growth of continental crust around the Junggar Basin, Xinjiang, China. Part I: timing of post-collisional plutonism. Acta Petrol. Sin. 22:1077–1086 (in Chinese with English abstract).

Han, Y., and Zhao, G. 2018. Final amalgamation of the Tianshan and Junggar orogenic collage in the southwestern Central Asian Orogenic Belt: constraints on the closure of the Paleo-Asian Ocean. Earth-Sci. Rev. 186:129–152.

He, G.; Han, B.; Yue, Y.; and Wang, J. 1990. Tectonic division and crustal evolution of Altay orogenic belt in China. Geosci. Xinjiang 2:9–20 (in Chinese with English abstract).

Holland, T., and Blundy, J. D. 1994. Non-ideal interactions in calcic amphiboles and their bearing on amphibole-plagioclase thermometry. Contrib. Mineral. Petrol. 116:433–447.

Hong, T.; Klemd, R.; Gao, J.; Xiang, P.; Xu, X.-W.; You, J.; Wang, X.-S.; Wu, C.; Li, H.; and Ke, Q. 2017. The tectonic evolution of the Irtysh tectonic belt: new zircon U-Pb ages of arc-related and collisional granitoids in the Kalaxiangar tectonic belt, NW China. Lithos 272–273:46–68.

Husen, A.; Kamenetsky, V. S.; Everard, J. L.; and Kamenetsky, M. B. 2016. Transition from ultra-enriched to ultra-depleted primary MORB melts in a single volcanic suite (Macquarie Island, SW Pacific): implications for mantle source, melting process and plumbing system. Geochim. Cosmochim. Acta 185:112–128.

Jahn, B.-M. 2004. The Central Asian Orogenic Belt and growth of the continental crust in the Phanerozoic. *In* Malpas, J.; Fletcher, C. J. N.; Ali, J. R.; and Aitchison, J. C., eds. Aspects of the tectonic evolution of China. Geol. Soc. Lond. Spec. Publ. 226:73–100.

Jian, P.; Kröner, A.; Jahn, B.-m.; Windley, B. F.; Shi, Y.; Zhang, W.; Zhang, F.; Miao, L.; Tomurhuu, D.; and Liu, D. 2014. Zircon dating of Neoproterozoic and Cambrian ophiolites in West Mongolia and implications for the timing of orogenic processes in the central part of the Central Asian Orogenic Belt. Earth-Sci. Rev. 133:62–93.

Jiang, Y.; Schulmann, K.; Kröner, A.; Sun, M.; Lexa, O.; Janoušek, V.; Buriánek, D.; Yuan, C.; and Hanžl, P. 2017. Neoproterozoic-early Paleozoic peri-Pacific accretionary evolution of the Mongolian Collage System: insights from geochemical and U-Pb zircon data from the Ordovician sedimentary wedge in the Mongolian Altai. Tectonics 36:2305–2331.

Jiang, Y.; Schulmann, K.; Sun, M.; Štípská, P.; Guy, A.; Janoušek, V.; Lexa, O.; and Yuan, C. 2016. Anatexis of accretionary wedge, Pacific-type magmatism, and

formation of vertically stratified continental crust in the Altai Orogenic Belt. Tectonics 35:3095–3118.

Jiang, Y.; Sun, M.; Zhao, G.; Yuan, C.; Xiao, W.; Xia, X.; Long, X.; and Wu, F. 2011. Precambrian detrital zircons in the early Paleozoic Chinese Altai: their provenance and implications for the crustal growth of central Asia. Precambrian Res. 189:140–154.

Khain, E. V.; Bibikova, E. V.; Salnikova, E. B.; Kröner, A.; Gibsher, A. S.; Didenko, A. N.; Degtyarev, K. E.; and Fedotova, A. A. 2003. The Palaeo-Asian ocean in the Neoproterozoic and early Palaeozoic: new geochronologic data and palaeotectonic reconstructions. Precambrian Res. 122:329–358.

Kruk, N. N.; Rudnev, S. N.; Vladimirov, A. G.; Shokalsky, S. P.; Kovach, V. P.; Serov, P. A.; and Volkova, N. I. 2011. Early–middle Paleozoic granitoids in Gorny Altai, Russia: implications for continental crust history and magma sources. J. Asian Earth Sci. 42:928–948.

Laurent-Charvet, S.; Charvet, J.; Monié, P.; and Shu, L. 2003. Late Paleozoic strike-slip shear zones in eastern central Asia (NW China): new structural and geochronological data. Tectonics 22:1009. doi:10.1029/2001TC901047.

Leake, B. E.; Woolley, A. R.; Arps, C. E. S.; Birch, W. D.; Grice, M. C.; Hawthorne, F. C.; Kato, A.; et al. 1997. Nomenclature of amphiboles: report of the subcommittee on amphiboles of the International Mineralogical Association, Commission on New Minerals and Mineral Names. Can. Mineral. 35:219–246.

Li, J.; Xiao, X.; and Chen, W. 2000. Late Ordovician continental basement of the eastern Junggar Basin in Xinjiang, NW China: evidence from the Laojunmiao metamorphic complex on the northeastern basin margin. Reg. Geol. China 19:297–302 (in Chinese with English abstract).

Li, P.; Sun, M.; Rosenbaum, G.; Cai, K.; Chen, M.; and He, Y. 2016*a*. Transpressional deformation, strain partitioning and fold superimposition in the southern Chinese Altai, Central Asian Orogenic Belt. J. Struct. Geol. 87:64–80.

Li, P.; Sun, M.; Rosenbaum, G.; Cai, K.; and Yu, Y. 2015*a*. Structural evolution of the Irtysh Shear Zone (northwestern China) and implications for the amalgamation of arc systems in the Central Asian Orogenic Belt. J. Struct. Geol. 80:142–156.

Li, P.; Sun, M.; Rosenbaum, G.; Jiang, Y.; and Cai, K. 2016*b*. Structural evolution of zonal metamorphic sequences in the southern Chinese Altai and relationships to Permian transpressional tectonics in the Central Asian Orogenic Belt. Tectonophysics 693:277–289.

Li, P.; Sun, M.; Rosenbaum, G.; Jourdan, F.; Li, S.; and Cai, K. 2017. Late Paleozoic closure of the Ob-Zaisan Ocean along the Irtysh shear zone (NW China): implications for arc amalgamation and oroclinal bending in the Central Asian orogenic belt. Geol. Soc. Am. Bull. 129:547–569.

Li, P.; Yuan, C.; Sun, M.; Long, X.; and Cai, K. 2015*b*. Thermochronological constraints on the late Paleozoic tectonic evolution of the southern Chinese Altai. J. Asian Earth Sci. 113:51–60.

Li, X.-H.; Li, Z.-X.; Wingate, M. T. D.; Chung, S.-L.; Liu, Y.; Lin, G.-C.; and Li, W.-X. 2006. Geochemistry of the 755 Ma Mundine Well dyke swarm, northwestern Australia: part of a Neoproterozoic mantle superplume beneath Rodinia? Precambrian Res. 146:1–15.

Li, X.-H.; Liu, Y.; Li, Q.-L.; Guo, C.-H.; and Chamberlain, K. R. 2009. Precise determination of Phanerozoic zircon Pb/Pb age by multicollector SIMS without external standardization. Geochem. Geophys. Geosyst. 10: Q04010. doi:10.1029/2009GC002400.

Li, X.-R.; Liu, F.; and Yang, F.-Q. 2012. Geological times and its significance of the two mica syenogranite in the Keyinblak Cu-Zn deposit area in Altay, Xinjiang. Xinjiang Geol. 30:5–11 (in Chinese with English abstract).

Li, Z.; Yang, X.; Li, Y.; Santosh, M.; Chen, H.; and Xiao, W. 2014. Late Paleozoic tectono-metamorphic evolution of the Altai segment of the Central Asian Orogenic Belt: constraints from metamorphic P-T pseudosection and zircon U-Pb dating of ultra-high-temperature granulite. Lithos 204:83–96.

Liu, W.; Liu, X. J.; and Xiao, W. J. 2012. Massive granitoid production without massive continental-crust growth in the Chinese Altay: insight into the source rock of granitoids using integrated zircon U-Pb age, Hf-Nd-Sr isotopes and geochemistry. Am. J. Sci. 312:629–684.

Long, X.; Sun, M.; Yuan, C.; Xiao, W.; and Cai, K. 2008. Early Paleozoic sedimentary record of the Chinese Altai: implications for its tectonic evolution. Sediment. Geol. 208:88–100.

Long, X.; Sun, M.; Yuan, C.; Xiao, W.; Lin, S.; Wu, F.; Xia, X.; and Cai, K. 2007. Detrital zircon age and Hf isotopic studies for metasedimentary rocks from the Chinese Altai: implications for the early Paleozoic tectonic evolution of the Central Asian Orogenic Belt. Tectonics 26:TC5015. doi:10.1029/2007TC002128.

Long, X.; Yuan, C.; Sun, M.; Safonova, I.; Xiao, W.; and Wang, Y. 2012*a*. Geochemistry and U-Pb detrital zircon dating of Paleozoic graywackes in East Junggar, NW China: insights into subduction-accretion processes in the southern Central Asian Orogenic Belt. Gondwana Res. 21:637–653.

Long, X.; Yuan, C.; Sun, M.; Xiao, W.; Wang, Y.; Cai, K.; and Jiang, Y. 2012*b*. Geochemistry and Nd isotopic composition of the early Paleozoic flysch sequence in the Chinese Altai, central Asia: evidence for a northward-derived mafic source and insight into Nd model ages in accretionary orogen. Gondwana Res. 22:554–566.

Long, X.; Yuan, C.; Sun, M.; Xiao, W.; Zhao, G.; Wang, Y.; Cai, K.; Xia, X.; and Xie, L. 2010. Detrital zircon ages and Hf isotopes of the early Paleozoic flysch sequence in the Chinese Altai, NW China: new constrains on depositional age, provenance and tectonic evolution. Tectonophysics 480:213–231.

Ludwig, K. R. 2003. Isoplot/Ex version 3.00, a geochronological toolkit for Microsoft Excel. Berkeley, CA, Berkeley Geochronology Center.

Lugmair, G. W., and Marti, K. 1977. Sm-Nd-Pu timepieces in the Angra dos Reis meteorite. Earth Planet. Sci. Lett. 35:273–284.

Maruyama, S. 1997. Pacific-type orogeny revisited: Miyashiro-type orogeny proposed. Isl. Arc 6:91–120.
Matsuda, T., and Uyeda, S. 1971. On the Pacific-type orogeny and its model—extension of the paired belts concept and possible origin of marginal seas. Tectonophysics 11:5–27.
McKenzie, D., and O'Nions, R. K. 1991. Partial melt distributions from inversion of rare earth element concentrations. J. Petrol. 32:1021–1091.
———. 1995. The source regions of ocean island basalts. J. Petrol. 36:133–159.
Miyashiro, A. 1974. Volcanic rock series in island arcs and active continental margins. Am. J. Sci. 274:321–355.
Niu, Y.; Collerson, K. D.; Batiza, R.; Wendt, J. I.; and Regelous, M. 1999. Origin of enriched-type mid-ocean ridge basalt at ridges far from mantle plumes: the East Pacific Rise at 11°20′N. J. Geophys. Res. Solid Earth 104:7067–7087.
O'Hara, K. D.; Yang, X.-Y.; Xie, G.; and Li, Z. 1997. Regional $\delta^{18}O$ gradients and fluid-rock interaction in the Altay accretionary complex, northwest China. Geology 25:443–446.
Pearce, J. A. 2008. Geochemical fingerprinting of oceanic basalts with applications to ophiolite classification and the search for Archean oceanic crust. Lithos 100:14–48.
Pearce, J. A., and Stern, R. J. 2006. Origin of back-arc basin magmas: trace element and isotope perspectives. *In* Christie, D. M.; Fisher, C. R.; Lee, S.-M.; and Givens, S., eds. Back-arc spreading systems: geological, biological, chemical, and physical interactions. Geophys. Monogr. Ser. 166. Washington, DC, American Geophysical Union, p. 63–86.
Pearce, T.; Gorman, B.; and Birkett, T. 1977. The relationship between major element chemistry and tectonic environment of basic and intermediate volcanic rocks. Earth Planet. Sci. Lett. 36:121–132.
Polat, A., and Hofmann, A. W. 2003. Alteration and geochemical patterns in the 3.7–3.8 Ga Isua greenstone belt, West Greenland. Precambrian Res. 126:197–218.
Polat, A.; Hofmann, A. W.; Münker, C.; Regelous, M.; and Appel, P. W. U. 2003. Contrasting geochemical patterns in the 3.7–3.8 Ga pillow basalt cores and rims, Isua greenstone belt, Southwest Greenland: implications for postmagmatic alteration processes. Geochim. Cosmochim. Acta 67:441–457.
Qi, L.; Hu, J.; and Gregoire, D. C. 2000. Determination of trace elements in granites by inductively coupled plasma mass spectrometry. Talanta 51:507–513.
Qu, G., and Zhang, J. 1991. Irtysh structural zone. Geosci. Xinjiang 3:115–131 (in Chinese with English abstract).
Ren, B.; Zhang, H.; Tang, Y.; and Lu, Z. 2011. LA-ICPMS U-Pb zircon geochronology of the Altai pegmatites and its geological significance. Acta Mineral. Sin. 31:587–596 (in Chinese with English abstract).
Rudnick, R. L., and Gao, S. 2003. Composition of the continental crust. *In* Rudnick, R. L., ed. The crust. Vol. 3 of Treatise on geochemistry. Amsterdam, Elsevier, p. 1–64.
Safonova, I. 2014. The Russian-Kazakh Altai orogen: an overview and main debatable issues. Geosci. Front. 5:537–552.
Safonova, I. Y.; Simonov, V. A.; Kurganskaya, E. V.; Obut, O. T.; Romer, R. L.; and Seltmann, R. 2012. Late Paleozoic oceanic basalts hosted by the Char suture-shear zone, East Kazakhstan: geological position, geochemistry, petrogenesis and tectonic setting. J. Asian Earth Sci. 49:20–39.
Salters, V. J. M., and Stracke, A. 2004. Composition of the depleted mantle. Geochem. Geophys. Geosyst. 5:Q05B07. doi:10.1029/2003GC000597.
Schilling, J. G. 1973. Iceland mantle plume: geochemical study of Reykjanes Ridge. Nature 242:565–571.
Schmidt, M. W. 1992. Amphibole composition in tonalite as a function of pressure: an experimental calibration of the Al-in-hornblende barometer. Contrib. Mineral. Petrol. 110:304–310.
Şengör, A. M. C.; Natal'in, B. A.; and Burtman, V. S. 1993. Evolution of the Altaid tectonic collage and Palaeozoic crustal growth in Eurasia. Nature 364:299–307.
Shen, P.; Pan, H.; Seitmuratova, E.; Yuan, F.; and Jakupova, S. 2015. A Cambrian intra-oceanic subduction system in the Bozshakol area, Kazakhstan. Lithos 224–225:61–77.
Shen, P.; Shen, Y.; Li, X.; Pan, H.; Zhu, H.; Meng, L.; and Dai, H. 2012. Northwestern Junggar basin, Xiemisitai Mountains, China: a geochemical and geochronological approach. Lithos 140:103–118.
Shinjo, R.; Chung, S.; Kato, Y.; and Kimura, M. 1999. Geochemical and Sr-Nd isotopic characteristics of volcanic rocks from the Okinawa Trough and Ryukyu Arc: implications for the evolution of a young, intracontinental back arc basin. J. Geophys. Res. Solid Earth 104:10,591–10,608.
Su, Y.; Zheng, J.; Griffin, W. L.; Zhao, J.; Tang, H.; Ma, Q.; and Lin, X. 2012. Geochemistry and geochronology of Carboniferous volcanic rocks in the eastern Junggar terrane, NW China: implication for a tectonic transition. Gondwana Res. 22:1009–1029.
Sun, C., and Liang, Y. 2013. The importance of crystal chemistry on REE partitioning between mantle minerals (garnet, clinopyroxene, orthopyroxene, and olivine) and basaltic melts. Chem. Geol. 358:23–36.
Sun, G.; Li, J.; Yang, T.; Li, Y.; Zhu, Z.; and Yang, Z. 2009*a*. Zircon SHRIMP U-Pb dating of two linear granite plutons in southern Altay Mountains and its tectonic implications. Geol. China 36:976–987 (in Chinese with an English abstract).
Sun, M.; Long, X.; Cai, K.; Jiang, Y.; Wang, B.; Yuan, C.; Zhao, G.; Xiao, W. J.; and Wu, F. 2009*b*. Early Paleozoic ridge subduction in the Chinese Altai: insight from the abrupt change in zircon Hf isotopic compositions. Sci. China Ser. D Earth Sci. 52:1345–1358.
Sun, M.; Yuan, C.; Xiao, W.; Long, X.; Xia, X.; Zhao, G.; Lin, S.; Wu, F.; and Kröner, A. 2008. Zircon U-Pb and Hf isotopic study of gneissic rocks from the Chinese Altai: progressive accretionary history in the early to middle Palaeozoic. Chem. Geol. 247:352–383.

Sun, S.-S., and McDonough, W. S. 1989. Chemical and isotopic systematics of oceanic basalts: implications for mantle composition and processes. *In* Saunders, A. D., and Norry, M. J., eds. Magmatism in the ocean basins. Geol. Soc. Lond. Spec. Publ. 42:313–345.

Taylor, B., and Martinez, F. 2003. Back-arc basin basalt systematics. Earth Planet. Sci. Lett. 210:481–497.

Tong, L.; Xu, Y.; Cawood, P. A.; Zhou, X.; Chen, Y.; and Liu, Z. 2014*a*. Anticlockwise P-T evolution at ~280 Ma recorded from ultrahigh-temperature metapelitic granulite in the Chinese Altai orogenic belt, a possible link with the Tarim mantle plume? J. Asian Earth Sci. 94:1–11.

Tong, Y.; Hong, D.; Wang, T.; Wang, S.; and Han, B. 2006*a*. TIMS U-Pb zircon ages of Fuyun post-orogenic linear granite plutons on the southern margin of Altay orogenic belt and their implications. Acta Petrol. Mineral. 25:85–89 (in Chinese with English abstract).

Tong, Y.; Wang, T.; Jahn, B.; Sun, M.; Hong, D.; and Gao, J. 2014*b*. Post-accretionary Permian granitoids in the Chinese Altai Orogen: geochronology, petrogenesis and tectonic implications. Am. J. Sci. 314:80–109.

Tong, Y.; Wang, T.; Kovach, V. P.; Hong, D. W.; and Han, B. F. 2006*b*. Age and origin of the Takeshiken postorogenic alkali-rich intrusive rocks in southern Altai, near the Mongolian border in China and its implications for continental growth. Acta Petrol. Sin. 22:1267–1278 (in Chinese with English abstract).

Tong, Y.; Wang, T.; Siebel, W.; Hong, D.-W.; and Sun, M. 2012. Recognition of early Carboniferous alkaline granite in the southern Altai orogen: post-orogenic processes constrained by U-Pb zircon ages, Nd isotopes, and geochemical data. Int. J. Earth Sci. 101:937–950.

van Westrenen, W.; Blundy, J. D.; and Wood, B. J. 2000. Effect of Fe^{2+} on garnet-melt trace element partitioning: experiments in FCMAS and quantification of crystal-chemical controls in natural systems. Lithos 53:189–201.

Volkova, N. I.; Travin, A. V.; and Yudin, D. S. 2011. Ordovician blueschist metamorphism as a reflection of accretion-collision events in the Central Asian orogenic belt. Russ. Geol. Geophys. 52:72–84.

Wan, B.; Xiao, W.; Windley, B. F.; and Yuan, C. 2013. Permian hornblende gabbros in the Chinese Altai from a subduction-related hydrous parent magma, not from the Tarim mantle plume. Lithosphere 5:290–299.

Wang, T.; Hong, D.; Jahn, B.; Tong, Y.; Wang, Y.; Han, B.; and Wang, X. 2006. Timing, petrogenesis, and setting of Paleozoic synorogenic intrusions from the Altai Mountains, Northwest China: implications for the tectonic evolution of an accretionary orogen. J. Geol. 114:735–751.

Wang, T.; Hong, D. W.; Tong, Y.; Han, B. F.; and Shi, Y. R. 2005. Zircon U-Pb SHRIMP age and origin of post-orogenic Lamazhao granitic pluton from Altai orogen: its implications for vertical continental growth. Acta Petrol. Sin. 21:640–650 (in Chinese with English abstract).

Wang, T.; Jahn, B.-M.; Kovach, V. P.; Tong, Y.; Hong, D.-W.; and Han, B.-F. 2009*a*. Nd-Sr isotopic mapping of the Chinese Altai and implications for continental growth in the Central Asian Orogenic Belt. Lithos 110:359–372.

Wang, W.; Wei, C.; Wang, T.; Lou, Y.; and Chu, H. 2009*b*. Confirmation of pelitic granulite in the Altai orogen and its geological significance. Chin. Sci. Bull. 54:2543–2548.

Wang, W.; Wei, C.; Zhang, Y.; Chu, H.; Zhao, Y.; and Liu, X. 2014*a*. Age and origin of sillimanite schist from the Chinese Altai metamorphic belt: implications for late Palaeozoic tectonic evolution of the Central Asian Orogenic Belt. Int. Geol. Rev. 56:224–236.

Wang, Y.; Long, X.; Wilde, S. A.; Xu, H.; Sun, M.; Xiao, W.; Yuan, C.; and Cai, K. 2014*b*. Provenance of early Paleozoic metasediments in the central Chinese Altai: implications for tectonic affinity of the Altai-Mongolia terrane in the Central Asian Orogenic Belt. Lithos 210–211:57–68.

Wang, Y.; Wang, J.; Wang, L.; Long, L.; Tang, P.; Liao, Z.; Zhang, H.; and Shi, Y. 2012. The Tuerkubantao ophiolite mélange in Xinjiang, NW China: new evidence for the Erqis suture zone. Geosci. Front. 3:587–602.

Waters, C. L.; Sims, K. W. W.; Perfit, M. R.; Blichert-Toft, J.; and Blusztajn, J. 2011. Perspective on the genesis of E-MORB from chemical and isotopic heterogeneity at 9–10°N East Pacific Rise. J. Petrol. 52:565–602.

Wilhem, C.; Windley, B. F.; and Stampfli, G. M. 2012. The Altaids of Central Asia: a tectonic and evolutionary innovative review. Earth-Sci. Rev. 113:303–341.

Wilson, M. 1989. Igneous petrogenesis: a global tectonic approach. London, Unwin Hyman.

Winchester, J. A., and Floyd, P. A. 1977. Geochemical discrimination of different magma series and their differentiation products using immobile elements. Chem. Geol. 20:325–343.

Windley, B. F.; Alexeiev, D. V.; Xiao, W.; Kröner, A.; and Badarch, G. 2007. Tectonic models for accretion of the Central Asian Orogenic Belt. J. Geol. Soc. Lond. 164:31–47.

Windley, B. F.; Kröner, A.; Guo, J.; Qu, G.; Li, Y.; and Zhang, C. 2002. Neoproterozoic to Paleozoic geology of the Altai Orogen, NW China: new zircon age data and tectonic evolution. J. Geol. 110:719–737.

Wood, D. A. 1980. The application of a Th-Hf-Ta diagram to problems of tectonomagmatic classification and to establishing the nature of crustal contamination of basaltic lavas of the British Tertiary Volcanic Province. Earth Planet. Sci. Lett. 50:11–30.

Workman, R. K., and Hart, S. R. 2005. Major and trace element composition of the depleted MORB mantle (DMM). Earth Planet. Sci. Lett. 231:53–72.

Wu, Y.; Yang, F.; Liu, F.; Geng, X.; Li, Q.; and Zheng, J. 2015. Petrogenesis and tectonic settings of volcanic rocks of the Ashele Cu-Zn deposit in southern Altay, Xinjiang, Northwest China: insights from zircon U-Pb geochronology, geochemistry and Sr-Nd isotopes. J. Asian Earth Sci. 112:60–73.

Xiao, W.; Han, C.; Liu, W.; Wan, B.; Zhang, J.; Ao, S.; Zhang, Z.; Song, D.; Tian, Z.; and Luo, J. 2014. How

many sutures in the southern Central Asian Orogenic Belt: insights from East Xinjiang–West Gansu (NW China)? Geosci. Front. 5:525–536.

Xiao, W.; Han, C.; Yuan, C.; Sun, M.; Lin, S.; Chen, H.; Li, Z.; Li, J.; and Sun, S. 2008. Middle Cambrian to Permian subduction-related accretionary orogenesis of northern Xinjiang, NW China: implications for the tectonic evolution of central Asia. J. Asian Earth Sci. 32:102–117.

Xiao, W.; Huang, B.; Han, C.; Sun, S.; and Li, J. 2010. A review of the western part of the Altaids: a key to understanding the architecture of accretionary orogens. Gondwana Res. 18:253–273.

Xiao, W.; Windley, B. F.; Han, C.; Liu, W.; Wan, B.; Zhang, J.; Ao, S.; Zhang, Z.; and Song, D. 2018. Late Paleozoic to early Triassic multiple roll-back and oroclinal bending of the Mongolia collage in Central Asia. Earth-Sci. Rev. 186:94–128.

Xiao, W.; Windley, B. F.; Sun, S.; Li, J.; Huang, B.; Han, C.; Yuan, C.; Sun, M.; and Chen, H. 2015. A tale of amalgamation of three Permo-Triassic collage systems in Central Asia: oroclines, sutures, and terminal accretion. Annu. Rev. Earth Planet. Sci. 43:477–507.

Xiao, W.; Windley, B. F.; Yuan, C.; Sun, M.; Han, C.; Lin, S.; Chen, H.; Yan, Q. R.; Liu, D. Y.; and Qin, K. 2009. Paleozoic multiple subduction-accretion processes of the southern Altaids. Am. J. Sci. 309:221–270.

Xu, X.; Li, X.; Jiang, N.; Li, Q.; Qu, X.; Yang, Y.; Zhou, G.; and Dong, L. 2015. Basement nature and origin of the Junggar terrane: new zircon U-Pb-Hf isotope evidence from Paleozoic rocks and their enclaves. Gondwana Res. 28:288–310.

Yang, T. N.; Li, J. Y.; Liang, M. J.; and Wang, Y. 2015. Early Permian mantle-crust interaction in the south-central Altaids: high-temperature metamorphism, crustal partial melting, and mantle-derived magmatism. Gondwana Res. 28:371–390.

Yuan, C.; Sun, M.; Xiao, W.; Li, X.; Chen, H.; Lin, S.; Xia, X.; and Long, X. 2007. Accretionary orogenesis of the Chinese Altai: insights from Paleozoic granitoids. Chem. Geol. 242:22–39.

Zhang, C.; Li, Z.; Li, X.; Xu, Y.; Zhou, G.; and Ye, H. 2010. A Permian large igneous province in Tarim and Central Asian orogenic belt, NW China: results of a ca. 275 Ma mantle plume? Geol. Soc. Am. Bull. 122:2020–2040.

Zhang, C.; Santosh, M.; Zou, H.; Xu, Y.; Zhou, G.; Dong, Y.; Ding, R.; and Wang, H. 2012. Revisiting the "Irtish tectonic belt": implications for the Paleozoic tectonic evolution of the Altai orogen. J. Asian Earth Sci. 52:117–133.

Zhang, C.; Zou, H.; Yao, C.; and Dong, Y. 2014. Origin of Permian gabbroic intrusions in the southern margin of the Altai Orogenic belt: a possible link to the Permian Tarim mantle plume? Lithos 204:112–124.

Zhang, Z.; Mao, J.; Cai, J.; Kusky, T. M.; Zhou, G.; Yan, S.; and Zhao, L. 2008. Geochemistry of picrites and associated lavas of a Devonian island arc in the northern Junggar terrane, Xinjiang (NW China): implications for petrogenesis, arc mantle sources and tectonic setting. Lithos 105:379–395.

Zhang, Z.; Zhou, G.; Kusky, T. M.; Yan, S.; Chen, B.; and Zhao, L. 2009. Late Paleozoic volcanic record of the eastern Junggar terrane, Xinjiang, northwestern China: major and trace element characteristics, Sr-Nd isotopic systematics and implications for tectonic evolution. Gondwana Res. 16:201–215.

Zheng, Y.-F., and Chen, R.-X. 2017. Regional metamorphism at extreme conditions: implications for orogeny at convergent plate margins. J. Asian Earth Sci. 145:46–73.

Zhou, G.; Zhang, Z.; Luo, S. B.; He, B.; Wang, X.; Yin, L. J.; Zhao, H.; Li, A. H.; and He, Y. K. 2007*a*. Confirmation of high-temperature strongly peraluminous Mayin'ebo granites in the south margin of Altay, Xinjiang: age, geochemistry and tectonic implications. Acta Petrol. Sin. 23:1909–1920 (in Chinese with English abstract).

Zhou, G.; Zhang, Z.; Wang, X.; Lou, S.; He, B.; and Zhang, X. 2007*b*. Zircon U-Pb SHRIMP and ^{40}Ar-^{39}Ar dating of the granitic mylonite in the Mayinebo fault belt of North Xinjiang and its geological significance. Acta Geol. Sin. 81:359–369 (in Chinese with English abstract).

Zhou, G.; Zhang, Z.; Wu, G.; Dong, L.; He, Y.; Dong, Y.; He, L.; Qin, J.; Zhao, Z.; and Liu, G. 2009. Postorogenic extension and continental growth of the northeastern margin of the Junggar: evidences from petrography and geochemistry of the Hadansun intrusive complex. Acta Geol. Sin. 83:331–346 (in Chinese with English abstract).

Zhou, J.-B.; Wilde, S. A.; Zhao, G.-C.; and Han, J. 2018. Nature and assembly of microcontinental blocks within the Paleo-Asian Ocean. Earth-Sci. Rev. 186:76–93.

Zonenshain, L. P.; Kuzmin, M. I.; and Natapov, L. M. 1990. Geology of the USSR: a plate tectonic synthesis. Geodyn. Ser. 21. Washington, DC, American Geophysical Union, 242 p.